Palacký University Olomouc
Faculty of Science
Department of Physical Chemistry

Insights into the interaction of transition metal atoms with defective graphene from DFT

Bachelor Thesis

Author:	Jan Navrátil
Supervisor:	Mgr. Piotr Błoński, Ph.D.

Study program:	Chemistry
Field of study:	Nanomaterial chemistry
Form of sturdy:	Full-time
Year:	2019

Declaration

I declare that I elaborated this bachelor thesis independently under the guidance of Mgr. Piotr Błoński, Ph.D. and thoroughly cited all used sources.

In Olomouc: …… ……

Handwritten signature

Acknowledgement

At first, I would like to express my gratitude to my supervisor Mgr. Piotr Błoński, Ph.D. In the beginning, he put much trust in me as a bachelor student without any deeper knowledge of quantum chemistry or linear algebra and agreed to lead me as his first bachelor student. He explained me the necessary basis of quantum chemistry and introduced me to VASP. He did not hesitate to answer my numerous questions. He recommended me many remarkable papers, and, in the end, he significantly helped me to polish the thesis to the final shape.

I would like to thank prof. RNDr. Michal Otyepka, Ph.D. who in the very beginning listened to my wishes and recommended me the direction of research that suited me the best. I also credit the support of doc. RNDr. Petr Jurečka, Ph.D., supervisor of our clusters, who helped me to solve some technical problems.

I express my gratitude to my partner Jana Poštolková who patiently listened to my extensive talks about quantum chemistry and this work and by her questions helped me to clarify many things. I would also like acknowledge my nanomaterial chemistry colleagues for our fruitful discussions.

Finally, I would like to thank my family and my friends for their support. In my free time, they helped me to relax and focus on different subjects than quantum chemistry. They also always kept cheering me up when thinks did not go well.

Bibliografické údaje

Autor:	Jan Navrátil
Název:	Pochopení interakce přechodných kovů s defektivním grafenem pomocí DFT
Typ závěrečné práce:	Bakalářská
Vedoucí práce:	Mgr. Piotr Błoński, Ph.D.
Rok prezentace:	2019
Katedra:	Katedra fyzikální chemie, Univerzita Palackého v Olomouci
Klíčová slova:	grafen, defektivní grafen, grafen s vakancemi, pyridinický dusík, atomy přechodných kovů, katalýza pomocí samostatných atomů, uchování dat pomocí samostatných atomů, adsorpční energie, DOS, Baderovy náboje, MAE, SOC, DFT
Počet stran:	53
Počet příloh:	2
Jazyk:	Anglický

Abstrakt: Techniky uchování dat pomocí jednotlivých atomů a katalýza pomocí samostatných atomů pro správnou funkci potřebují specifickou pozici, která by pevně uchytila "aktivní" atomy a zabránila jim ve shlukování. Tato teoretická bakalářská práce ukazuje, že adsorpce vybraných atomů přechodných kovů (Fe, Co, Ni, Ru, Rh, Pd, Os, Ir, Pt) do defektů v defektivním grafenu (jedna vakance, jedna vakance dekorovaná pyridinickými dusíky, dvojvakance, dvojvakance dekorovaná pyridinickými dusíky) je energeticky výhodná, ve spoustě případů byla vazba silnější než 5 eV. Zatímco atomy Pt jsou na čistém grafenu poměrně mobilní, vakance ukotvují adatom silněji než pozice vzdálenější od defektu. Strukturní, elektronické a magnetické vlastnosti byly pečlivě analyzovány. Trendy ve vypočtených charakteristikách byly prozkoumány a byla vypočtena jejich korelace s adsorpční energií. Relativistické nekolineární kalkulace ukázaly významné hodnoty magnetické anizotropní energie IrDVG (~ 7 meV) s jednoduchou osou magnetizace kolmou na rovinu grafenu. Opačným případem je IrSVNG, kde je jednoduchá osa paralelní s rovinou grafenu oproti ose kolmé na rovinu grafenu preferována o ~ 10 meV. Vlastnosti obou systémů jsou diskutovány na základě relativistických elektronických struktur.

Bibliographic Identification

Author:	Jan Navrátil
Title:	Insights into the interaction of transition metal atoms with defective graphene from DFT
Type of thesis:	Bachelor
Supervisor:	Mgr. Piotr Błoński, Ph.D.
Year of presentation:	2019
Department:	Department of Physical Chemistry, Palacký University Olomouc
Keywords:	graphene, defective graphene, vacancy graphene, pyridinic nitrogen, transition metal atoms, single atom catalysis, single atom data storage, adsorption energy, DOS, Bader charges, MAE, SOC, DFT
Number of pages:	53
Number of appendices:	2
Language:	English

Abstract: Single atom data storage and single atom heterogenous catalysis need for proper function specific position that thoroughly holds the concerned "active" atoms and prevents them from clustering. Presented theoretical thesis shows that adsorption of selected transition metal atoms (Fe, Co, Ni, Ru, Rh, Pd, Os, Ir, Pt) to defects in defective graphene (single vacancy, single vacancy decorated by pyridinic nitrogen atoms, divacancy, divacancy decorated by pyridinic nitrogen atoms) is energetically favourable, in many cases the binding is stronger than 5 eV. While Pt atoms at pristine graphene are rather mobile, vacancies anchor the adatom rather strongly, compared to the positions farther from the defect. Structural, electronic and magnetic properties were thoroughly analysed. Trends in the calculated characteristics were inspected and correlation with adsorption energy was evaluated. Relativistic non-collinear calculations showed remarkable magnetic anisotropy energy of IrDVG (~ 7 meV) with easy axis perpendicular to graphene plane. Contrary to this, magnetic axis perpendicular to the graphene plane of IrSVNG is disfavoured by ~ 10 meV in comparison with easy magnetic axis parallel to the graphene layer. Properties of both systems are discussed based on the relativistic electronic structures.

Table of Contents

Introduction

Nearly everybody knows that everything around us consists of atoms, but it is not a long time ago when people started to be able to observe and work with single atoms. Important milestone was famous visionary lecture "There's Plenty of Room at the Bottom" [1] held in 1959 by Richard Feynman, where he sketched his hope of manipulating single atoms and creating useful devices of them. These thoughts are now considered as basis of nanotechnology. Development of advanced laboratory techniques – transmission electron microscopy (TEM) allowed scientists to achieve atomic resolution, in addition scanning tunnelling microscopy (STM) and atomic force microscopy (AFM) added the possibility to manipulate with single atoms along the surface. At the same time the rapid development of computers performance allowed researchers to carry out quantum chemistry calculations of model systems representing real systems with very good precision. Both approaches are today on an equal footing – (a) quantum chemistry calculations can describe why synthesized substance has right those properties when precise geometry of it is known, or (b) theoretical calculations can predict materials with interesting features in advance and after that the information is passed to research chemists in laboratory that thereafter examine the properties in real conditions.

The past decade has witnessed a large increase of digital information amount, the actual trend is to double the existing amount of data every second year. It was predicted that from 2005 to 2020 the saved data will be multiplied 300 times.[2] The actual development of hard disk drives (HDDs) does not follow the famous Moore's law which states that the areal density of HDDs will double every second year.[3] It is clear, that if the number of HHDs would be constant, the gap between storage demand and actual capacity would constantly spread. In addition, in year 1999 Roger Wood[4] predicted, that information density limit is in order of 1 Tb / in^2, that means 155 Gb / cm^2. To continue with its enhancement, new approaches therefore have to come. Review paper by Shiroishi *et al.*[5] summarizes possibilities how to reach 1 Tb / in^2 limit and also go beyond it – bit patterned magnetic recording, heat assisted magnetic recording, microwave assisted magnetic recording, shingled writing recording and two dimensional magnetic recording. All the techniques somehow modify the writing and reading process, but they all strongly depend on the bit patterned medium (BPM) – the material which should keep the information. For achieving the highest

densities, there are very strict criteria – the magnetic centres must be placed in perfect lattice, must be independent of the others and their magnetic moment has to be stable enough to resist random thermal excitations.

Searching for material suitable for use as BPM became very important. To achieve highest information density, it is useful to start from the smallest imaginable particles that could store and preserve information – single metal atoms, dimers of transition metals or single molecules placed on suitable substrates. This work is focused on the single atoms of transition metals anchored to graphene.

Important quantity of the systems is magnetic anisotropy energy (MAE) which influences the information stability. In the gas phase, a transition-metal (TM) dimer is the smallest object showing magnetic anisotropy. Due to the spherical symmetry, single atoms do not show any magnetic anisotropy, their MAE is zero. However, binding TM atoms to a suitable surface or matrix breaks the symmetry and could set the ultimate limit of data storage to a single-atom magnetic bit. Just to briefly mention success in this field, Natterer *et al.*[6] practically showed that single Ho atom placed on MgO substrate can hold information bit that is stable for several hours and can be read remotely. Baltic *et al.*[7] prepared well-ordered superlattice of Dy atoms located on graphene grown on Ir(111). They report information density of 115 Tb/inch^2. Theoretical investigations of Błoński and Hafner[8–10] showed that heteroatomic dimer Ir-Co placed on graphene sheet on Cu(111) has MAE of 204 meV which would prevent loss of information at temperatures greater than room temperature.

For real applications, atoms or dimers placed on the surface of graphene must be bound strongly to some particular position to prevent the atoms from clustering. Gan *et al.*[11] showed that the barrier for Pt adatoms' movement on pristine graphene is low and the Pt adatoms are rather mobile. Defects in graphene can be created unintentionally during preparation of pristine samples or completely deliberately. Their presence in graphene could serve as anchoring centre for TM adatom. The aim of this theoretical work is to embed transition metal atoms of VIII B group of periodic table of elements to the defective graphene – single vacancy graphene, single vacancy pyridinic graphene, double vacancy graphene and double vacancy pyridinic graphene. Systems' geometry and adsorption energy have been examined as well as electronic properties like density of states (DOS), Bader charges and magnetic properties including magnetic anisotropy energy (in selected systems). This work also serves

as basis for future work when second metal atom will be added to examine its influence mainly on the systems' magnetic properties.

One should also note that TM adatoms anchored on graphene surface could be also important for single-atom heterogenous catalysis (SAHC), which is without doubt very important part of many chemical processes in laboratories as well as in the industry. Indeed, recent papers (for instance by Bakandritsos *et al.*[12]) show current interest in using graphene as basis for SAHC. Much information from this field provides review paper by Yang *et al.*[13] Numerous reasons of SAHCs' advantage exist, the most important are following - (a) single atoms catalysts have always the same geometry of used catalytic centre, (b) unsaturated bonds lead to enhanced activity, (c) quantum effects playing very important role can be also well tuned. Aim of many referred papers (as geometry comparison in the subchapter of geometry results) was indeed theoretical description of catalytic activity of the systems. This thesis aims to explain some observed systematic geometrical trends in these systems.

1 Theoretical Background

1.1 Modern Approaches to Information Storage, Limits and Solutions

Nowadays, information in personal computers is mostly saved in hard disk drives (HDDs) or solid-state drives (SSDs). Both drives use different approaches – HDDs contain magnetic media that holds the information and magnetic head that reads and writes the information. The HDDs contain rotating parts which are their biggest disadvantage.[14] Information in SSDs is saved in integrated circuits and they do not contain any moving parts.[15]

SSDs overcome HDDs in their reading speed of scattered information (random access), they also consume less energy and are very resistant to damage caused by their movement while they are working. SSDs are often lighter and smaller and in principle they are completely silent. On the other hand, HDDs are still much cheaper in meaning cost per one GB and they should not loose stored information after years of inactivity (but mechanical problems with rotating parts could occur).[15] In 2016, common information density in HDDs was 1.1 Tb / in^2, for SSDs 2.0 Tb / in^2.[3]

HDD contains rotating disks called platters. The basis of platter is nonmagnetic material (earlier aluminium alloy, now glass or ceramic).[14] Grains of ferromagnetic material – typically Co-Cr-Pt alloy with some admixture – are placed on the platter's surface. The grains are separated by nonmagnetic material.[16] After manufacturing, grains are distributed with some irregularities[17] therefore disks are designed to have more grains holding one information bit.[4] The second important part is access arm with reading and writing head – one head for one side of platter. Proper combination of access arm angle and phase of platter rotation allows the head to access all points on the platter. Operating distance of the head is in the order of ten nanometres above the surface.[14]

Wood showed in his paper[4] that simple scaling of size-dependent bit volume (a product of multiplication of read width, bit length and thickness of the medium) can predict highest information densities in classical HDDs of about 1 Tb / in^2. For information stability over years the superparamagnetic effect plays very important role - it can cause the flip of magnetization due to the random thermal excitations, so it needs to be minimized. Wood derived that the lower limit of grain size to avoid superparamagnetic regime is about 10 nm in diameter. Very important parameter is also signal to noise ratio (SNR) which defines

reliability of reading process. If the size of grain is kept at the lowest possible value to resist superparamagnetic effect, SNR of magnetic media scales with cube of linear scaling factor. SNR of the head scales in linear or square proportion of linear scale factor (depending on included criterion). Either way, SNR of magnetic media seems to be greater problem. Another problem is the above-mentioned distribution of grains, Wood suggests using 5 grains to store one information bit as reasonably safe option.

Some ways how to break the information density limit of 1 Tb / in^2 are presented in the review paper by Shiroishi *et al.*[5] The first option is to use bit-patterned magnetic recording (BMPR). One bit would be stored in one very well-defined magnetic island. The islands would have exactly the aimed size to be able to contain information bit with reasonable stability but not to be unnecessarily large. Islands would be also very well ordered on the surface of platter. Those properties would allow to achieve higher densities of the islands as well as would minimize the noise from neighbour islands during reading. The highest disadvantage comes from the need for an absolutely precise timing – the reading and writing would have to be done when the head would be exactly above the island. It was shown that this technique could reach information density of about 4 Tb / in^2, this should be also limit when energy assisted recording is not used. Its creating process would also contain many new steps like electron beam patterning and self-assembly of polymers. BPM is the basis of all new high-density approaches as it allows higher SNR and thermal stability as compared to the presently used media grains. However, both mass fabrication of BPM and its integration to the existing recording system of HDDs is considered to be the greatest challenge for its widespread commercial use. Finding suitable basis for BPM is also aim of this work – the matrix would be defective graphene, the magnetic materials would be formed by a regular array of TM adatoms.

If the magnetic islands in BPM would be so close to each other, it is possible that magnetically harder materials would have to be used to reliably save the information. In those cases, some additional energy would need to be used during writing to change the magnetic moment orientation. Energy could be delivered by heat (HAMR) or by microwaves (MAMR). Combination of HAMR with BPM could lead to enormous densities of 100 Tb / in^2.

1.2 Magnetism of Selected Systems Containing Atom or Dimer with Remarkable Magnetic Properties

As was mentioned in the introduction, the main interest of this thesis lies in the smallest systems that have two stable orientations of their magnetic moment with energetic barrier between them high enough to preserve the moments from spontaneous switching due to superparamagnetic effect. The height of barrier should be at least 30 meV, as it corresponds to the energy of thermal excitations of 80 °C. These materials could serve as BPM for new HDD-like nano-devices, or, at least, they could point out which properties are important for those features. In this chapter, interesting experimentally prepared materials are described at first, the second part is devoted to the systems that were theoretically predicted to be magnetically remarkable.

1.2.1 Experimentally prepared systems with magnetic atoms on surfaces

Single atoms placed on specific surface should provide good starting point for information storage devices as they are similar to the present materials used in HDD platters - solid material with specific surface could serve as support, the metal atoms would hold the information.

Baltic *et al.*[7] showed strategy how to create highly ordered lattice of Dy atoms carrying magnetic moments. They used Ir(111) surface covered by a single layer of graphene and thus creating moiré pattern. If temperature during Dy atom deposition was at about 40 K, Dy atoms were diffusing over graphene until reached very advantageous position – C-ring placed directly above Ir atom. Following this approach, they were able to prepare highly ordered system with Dy adatom every 10 x 10 graphene unit cells. If temperatures during deposition were lower than 10 K, the Dy atoms stayed in random C-rings, independently on the moiré pattern. Hysteresis loops measured both on ordered and unordered system were very similar, magnetism thus origins from Dy atoms alone, not from the interaction between them, and position of C-ring containing Dy atom in moiré pattern has also no influence. This system seems to be resistant against quantum tunnelling, so authors measured quite long magnetic lifetimes (about 1000 s at 2.5 K). Authors supported their results by theoretical calculations. They found that their system has barrier to magnetism reversal of 21.4 meV, but also contains one possible path for quantum tunnelling at 5.6 meV and thus observed information lifetimes are significantly shortened in comparison

to the ideal systems where the only path would be over the full barrier. Moreover, they proposed explanations of observed behaviour. At first, the higher the symmetry of adatom surroundings, the fewer paths for quantum tunnelling – in their case the magnetic centre had C_{6v} symmetry. At second, graphene acts like filter and strongly limits energy exchange between Ir(111) and Dy adatom. Further, the interaction between Ir(111) and graphene creates energy gap at E_F of graphene and, consequently, transition of conducting electrons between Ir(111) and Dy adatom is suppressed. As the last step they proofed that omitting of one single criterion leads to significant reduction of magnetic relaxation time.

Donati *et al.*[18] grew few thin MgO(100) films on Ag(100) surface a placed single Ho atom on its surface. They observed dependence of relaxation times on the thickness of the MgO layer. They measured hysteresis up to 30 K. Reported reasons for such high temperatures are similar to the above-mentioned research. They observed nearly identical relaxation times (approximately 26 minutes) at 10 K and 2.5 K and therefore they assume that at temperatures under 10 K the relaxation is led primarily by non-thermal processes. When temperature was at about 20 K, the relaxation time was approximately 11 minutes. Dependence of hysteresis on the number of MgO monolayers was also examined – it was shown that 3.6 monolayers are the lower limit for decoupling of adatom from electron and phonon bath of Ag and thus hysteresis to be observable.

Natterer *et al.*[6] used the same system as in Ref. [18] and examined the stability of magnetically saved information by two independent paths – locally using tunnel magnetoresistance and remotely using electron spin resonance (ESR) of neighbouring Fe atom. They wrote the information placing scanning tunnelling microscopy (STM) tip above Ho atom and applying voltage pulses until change in magnetoresistance was observed. After that they measured ESR spectra of Fe atom acting as sensor – magnetic moment presented at Fe is aligned with external magnetic field but quantity of absorption frequency shift is dependent of the neighbouring Ho atom due to the Zeeman splitting. If magnetic moment presented at Ho is parallel to the external magnetic field, the adsorption frequency shifts to lower frequencies and *vice versa*. They also showed that width of splitting depends of the distance between Ho and Fe atoms. According to this knowledge they prepared system where two atoms of Ho were placed in neighbourhood of the Fe atom, but distances between Ho atoms and Fe atom were different and, indeed, they were able to measure 4 different spectra according to the orientation of magnetic moment of Ho atoms. The closer

Ho atom, obviously, had higher impact on the peak position, the second one just slightly shifted it. They also reported that information remained stable for hours at temperature of 4.3 K, they were not able to examine properties at higher temperatures as their equipment was not suitable for it. Their work is clearly illustrated in Fig. 1 reprinted from paper[19] by Roberta Sessoli.

Natterer *et al.*[20] then continued examining the same system. They derived that the height of energy barrier between two stable states is 9.36 meV. They also measured the stability at higher temperatures and constant magnetic field of 8 T. The information was "written" to the energetically less favourable state (with opposite direction to the external magnetic field) and time until it switches to the more favourable state was measured. They found out that at 35 K the information should be stable as they did not observe spontaneous switching for 5 minutes. At 45 K spontaneous switching started to be significant, at 50 K the atoms irreversibly moved to the different positions where they lost their interesting magnetic properties. Although the single-atom information storage is possible, there are still many obstacles to overcome to have real applications. Those experiments were performed in an ultrahigh vacuum and at very low temperatures.

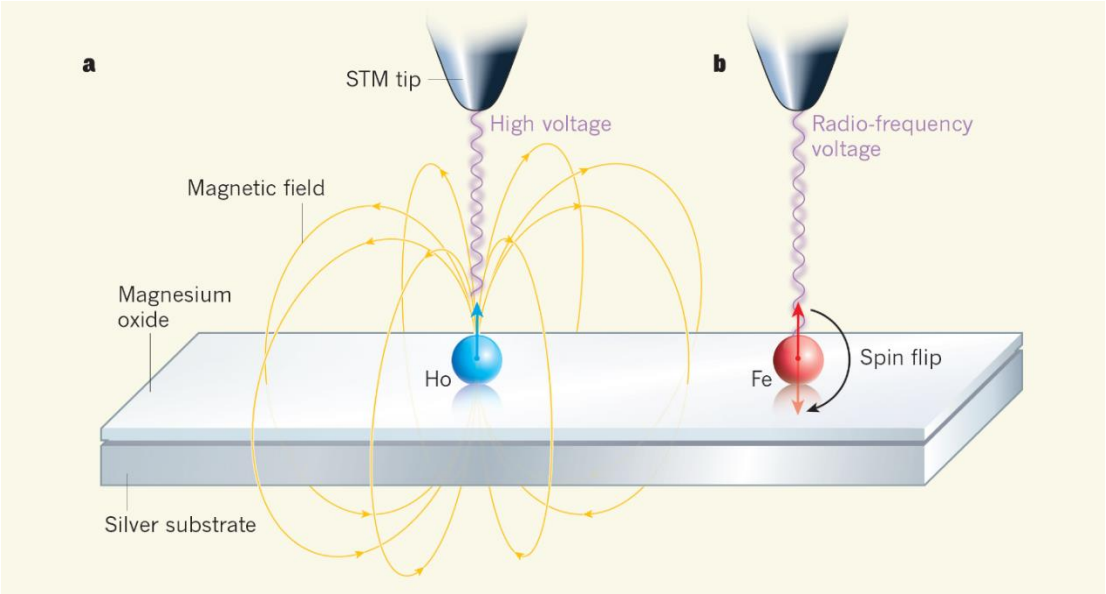

Fig. 1: Illustration of experiment by Natterer *et al.*[6] where they demonstrated writing and reading of information saved in single Ho atom. Information is written to Ho atom by applying voltage pulses from STM tip. Information is then remotely read using ESR, Fe atom acts as local magnetometer. Reprinted from "Single-atom data storage" [19], by R. Sessoli, 2017, *Nature*, *vol. 543*, 189. Copyright 2017 Nature.

1.2.2 Theoretically investigated systems with significant magnetic properties

Another approach is to design systems theoretically and examine their properties when placed on real substrates. The quantity of central interest is MAE – difference between total energies of systems with magnetic moment along hard and easy axis. MAE should thus correspond to the energetic barrier for switching of magnetic moments between two magnetic axes. DFT calculations for homoatomic dimers of VIII B group elements revealed[8] that some dimers have large MAEs exceeding 45 meV, namely Ir_2 (69.8 meV), Rh_2 (47.3 meV) and Pt_2 (46.3 meV). Analysis of spin-orbit coupling (SOC) on the Kohn-Sham eigenvalue spectra elucidated that physical mechanism responsible for the high MAE is the two-fold degeneracy of a singly occupied state at E_F for magnetization perpendicular to the dimer axis that is lifted for an axial magnetization.

Atoms of 3d elements have large magnetic moments, but negligible SOC, which is crucial for large MAE values. On the other hand, 5d elements are non-magnetic in bulk state, but have significant values of SOC and can become magnetic in small clusters. The substitution of Ir by Co in the Ir dimer keeps the large MAE of ~ 70 meV [9] of Ir_2. Moreover, mentioned elements are often included in alloys that are presently used in HDDs as magnetic media. Importantly, using of DFT for these systems is reasonable choice, as it gives similar results to reference quantum-chemistry (configuration-interaction) methods. Furthermore, for homoatomic dimers (Ir_2 and Pt_2) adsorbed on graphene significant reduction of MAE was found for Pt_2 (12 meV) and complete vanishing of MAE in case of Ir_2. For dimer of Ir-Co adsorbed on freestanding graphene with Co atom placed above the centre of the six-fold hole and Ir atom in upward position above it an enormous MAE of 93 meV was reported[9]. Although total magnetic moment remained nearly unchanged, significant changes in local spin and orbital moments were observed. Spin moment of Co atom was reduced, and orbital moment nearly disappeared. On the other hand, bond in dimer was weakened and elongated and thus Ir atom got more free-atom-like attributes. Its spin and orbital moments remarkably enhanced, and it became the centre of magnetic anisotropy of the system, magnetic moment anisotropy was 1.3 μ_B.

For real application the graphene layer must be placed on solid substrate. Theoretical DFT calculations[10], showed that Ir-Co dimers supported on Cu(111) surface in an upright geometry (Ir atom up) exhibit remarkable MAE of 204 meV. Cu(111) was chosen

as the substrate, as graphene grown on it is practically known to be high-quality. It was found that the most important source of MAE in case of Ir-Co is the doubly-degenerate (during perpendicular orientation of magnetic moment) orbital located at E_F occupied by single electron. When orientation of magnetic moment changes to parallel to the dimer axis, it splits under SOC conditions.

1.3 Graphene

Graphene is allotrope of carbon in which carbon atoms are placed in the perfect hexagonal lattice nearly in the plane. From classical point of view, it is a single sheet of graphite. This thought also led to its first preparation – Andre Geim and Konstantin Novoselov used adhesive tape to remove few carbon layers from highly organized graphite. After that they repeatedly used the tape to achieve preparing of layer with thickness of just single atom.[21] Their discovery restored the interest of many scientists in the field of 2D materials. For instance, Ashton *et al.*[22] predicted existence of more than 800 other materials that could be stable in just 2 dimensions.

Single C atom has 4 valence electrons. In graphene, C atoms are sp^2-hybridized. Each atom is connected to three other C atoms via σ-bonds, the whole structure is similar to honeycomb. 1 electron is, in model case, left in the p_z orbital. Actually, those orbitals of all C atoms hybridize together and create π-delocalized system. The Bravais lattice consist of two triangular sublattices, unit cell thus contains two C atoms. Distance between two neighbouring C atoms is 1.42 Å.[23]

Graphene is material that is for its unique properties frequently described as the material of the future. Various resources state that it is the strongest measured material[24], good thermal conductor even if its measured values significantly vary[25,26] and excellent electric conductor[27]. Actually, it was shown that graphene is actually zero-band-gap semiconductor, moreover, the electronic bands have shape of cone, and thus electrons behave like massless fermions.[23] Pristine graphene is diamagnetic.[28] Graphene also has high value of optical transmittance.[23] Moreover, derivatives of graphene can have completely different properties, for instance fluorographene is considered to be the thinnest prepared insulator.[29] Graphene and its derivatives have one of the highest specific surface area among all materials, therefore they show strong potential as catalysts.[30] Its other advantageous properties are strong ballistic transport, long spin lifetime and weak spin-orbit coupling,[23] which are demanded in spintronics – field of electronics where not just electron itself, but also its spin is used

to transfer and process the information. If suitable derivatives would be found, the electronic devices could be significantly improved.[31] From other fields of interest the following should be mentioned: electronics, energy storing and generating, optics, medicine, environment-treating technologies, *etc.* The most pronounced problem of application is the synthesis of pure graphene in large scales.[23] In the next subchapters, graphene with vacancies and graphene doped with nitrogen atoms will be presented, as they present the basis for systems studied in this work.

1.3.1 Graphene with vacancies

All information of graphene with vacancies are well summarized in the review paper by Tuček *et al.*[23] Vacancy is in principle created, when one or more carbon atoms are removed from the perfect graphene. In this work we focus on single vacancy graphene (SVG) and divacancy graphene (DVG). When one carbon atom is removed, the created single vacancy is surrounded by 3 dangling bonds. This state is energetically unfavourable, so 2 surrounding carbon atoms can form 1 single bond leaving just one dangling bond in the system. The total formation energy of reconstructed system from the perfect graphene is about 7.4 – 7.8 eV. The newly created bond is much longer (length about 2 Å) than other bonds in graphene. Both cases (1 and 3 dangling bonds) were predicted theoretically and also detected using special technique of high-resolution transmission electron microscopy (HRTEM). Vacancies can diffuse with barrier of 0.9 – 1.7 eV, although it was not observed during experiments. The situation is different, when 2 or more vacancies are presented in the system. If two single vacancies are very close, they can merge and create divacancy.

Presence of the single vacancy induces magnetism in the system. The source of magnetism is particularly the dangling bond. DOS analysis showed that two non-symmetric localized p_z states are presented at E_F. Value of the magnetic moment is 1 – 2 μ_B and depends on the used calculation functional. Magnetism of single vacancies was also confirmed by STM.

Divacancies can be formed by removing two carbon atoms or by merging two single vacancies as mentioned above. After such creation 4 dangling bonds exist there and the system commonly undergoes the relaxation process via forming 2 new single bonds, similarly as in the case of single vacancy. This structure is called V_2(5-8-5) – the numbers denote the number of carbon atoms in the newly created rings. The system can also be reconstructed in different ways, for instance by creating energetically more favourable

structure V_2(555-777). Both structures were confirmed using HRTEM. Formation energy of the whole divacancy is approximately 8 eV, only slightly higher than in the case of single vacancy, meaning that removal of the second atom from single vacancy costs nearly no energy. This is probably due to the presence of the dangling bond in the single vacancy system. The diffusion barrier is much higher (about 7 eV) causing that divacancies do not move.

Additional information about relaxed V_2(5-8-5) divacancy graphene is summarized in paper by Dai *et al.*[32] The newly created bonds are 1.8 Å long, the distance between these bonds is 3.1 Å. Density of states of resulting structure is completely symmetrical, consequently, the system is nonmagnetic.

1.3.2 Graphene with vacancies decorated by pyridinic nitrogen atoms

Structure and magnetic properties of single vacancy graphene with pyridinic nitrogen atoms around the single vacancy (SVNG) and graphene with divacancy decorated by pyridinic nitrogen atoms (DVNG) was theoretically studied by Fujimoto and Saito.[33] For SVNG they found that bonds between nitrogen atom and surrounding carbon atoms are shorter than common C-C bond in perfect graphene (1.33 Å x 1.42 Å) and that system preserves D_{3h} symmetry in contrast to the single vacancy graphene. They reported magnetic moment of 0.89 μ_B. In DVNG C-N bonds of similar length as in SVNG are presented. This means that nitrogen atoms are shifted farther from the other nitrogen atoms, in contrast to DVG where carbon atoms moved closer and created new single bonds. Hou *et al.*[34] confirm this behaviour and report that the distance of closer nitrogen atoms is 2.64 Å. Fujimoto and Saito[33] state that DVNG is nonmagnetic.

Stability and thermodynamics of creation of SVNG and DVNG was theoretically examined by Hou *et al.*[35] They found that substitution of carbon atom by nitrogen atom in pristine graphene is energetically unfavourable (0.785 eV) and the reluctance increases with increasing number of substituted atoms and (generally, but with some exceptions) with decreasing distance between nitrogen atoms. Situation is completely different if defects are presented. If just one carbon atom should be replaced, the most favourable is the one with dangling bond. In the case of two substituted atoms, the second nitrogen atom would be placed in the corner farthest from the vacancy of the five-membered ring. In the case of triple substitution, the most favourable and stable is the SVNG geometry described above

in this subchapter. Furthermore, the SVNG has smaller formation energy than SVG, meaning that the substitution should be exothermic. In divacancy (585) systems, with two substituted atoms the nitrogen atoms tend to occupy one side of the 8-membered ring, leaving the opposite reconstructed bond preserved. Substitution of 4 atoms and thus creating the DVNG structure (as was described above) is also favourable. This structure is, similarly as in the case of SVNG, energetically more advantageous than DVG.

The above-mentioned theoretical predictions were practically confirmed by Lin *et al.*[36] They grew layer of graphene by chemical vapour deposition of methane on Cu foil. After transferring graphene layer onto SiO_2 / Si substrate, they bombarded it by gas mixture of N_2 and O_3 (1:1). Following this procedure, they observed few C → N substitutions, but much more substitutions leading to formation of pyridinic N around single vacancy (with $n_N = 1 – 3$), or around divacancy ($n_N = 4$). Total number of single vacancies in region 50 nm x 50 nm was greater than 60. They also showed that these vacancies strongly attract transition metal atoms – they spontaneously and easily moved into the vacancy, but there they remained single. Ref. [36] is very important for the aims of this work, as it shows that preparation of systems similar to the currently examined systems in real conditions is indeed possible.

1.4 Theoretical part

At first, Born-Oppenheimer approximation, variational principle and pseudopotentials are presented. The centre of gravity of this work are DFT calculations so greater attention is devoted to DFT, its drawbacks and also ways to overcome them. Plane-wave approach is then presented as well as introduction of k-points. All information included in this chapter come from the book *Theoretical Surface Science* by Axel Groß.[37]

1.4.1 Born-Oppenheimer approximation, variational principle, pseudopotentials

For description of the ground state of examined system, the basis of quantum chemistry is the time-independent Schrödinger equation:

$$H\Psi(r) = E\Psi(r) \qquad (1)$$

where H stands for Hamiltonian, $\Psi(r)$ for wave function and E for energy eigenvalues. If also relativistic effects are considered, the wave function provides the most accurate description of ground-state so far. Schrödinger equation is so complex that it is possible to solve it

analytically just for few very simple cases. Even numerical solution is very demanding as the number of unknowns in differential equations being solved scales with 3 x number of electrons. Many approximations thus have to be included to make the calculation tractable.

One of the most successful approximations is Born-Oppenheimer (BO) approximation, sometimes called as adiabatic approximation. It follows the observations that atomic nuclei have mass that is 4 or 5 orders higher than the mass of electrons. If electrons and nuclei had the same kinetic energy, the velocity of electrons would be 2 or 3 orders higher than the velocity of nuclei. Electrons thus easily and immediately follow the movement of nuclei. One could then imply that electrons find ground state for any position of nuclei. At the same time, electronic configuration determines potentials in which nuclei move. The full Hamiltonian (H, Eq. 2) is thus divided to two branches. At first, electronic Hamiltonian (H_{el}, Eq. 3) enters the calculations with fixed nuclei coordinates (acting as parameters, not variables), at second, nuclei Hamiltonian (H_{nucl}, Eq. 4) can be similarly derived:

$$H = T_{nucl} + T_{el} + V_{nucl-nucl} + V_{nucl-el} + V_{el-el} \quad (2)$$

$$H_{el} = T_{el} + V_{nucl-el} + V_{el-el} \quad (3)$$

$$H_{nucl} = T_{nucl} + V_{nucl-nucl} + V_{nucl-el} \quad (4)$$

In the above-mentioned equations, T stands for kinetic part of Hamiltonian, V for electric potential part. Quantum effects of nuclei motions are often neglected, and classical equation of motion for nth nuclei is used instead

$$M_n \frac{\partial^2 R_n}{\partial t^2} = -\frac{\partial E_{el}}{\partial R_n} \quad (5)$$

where E_{el} stands for eigenenergy of electronic Hamiltonian, it is also called BO energy surface, M_n and R_n are mass and coordinates of nth nuclei respectively. BO approximation introduces negligible errors to the ground state calculations but can lead to very inaccurate solutions of excited state calculations.

In existing computational codes, the BO approximation is implemented as following scheme – the self-consistent electronic loop is performed for fixed ionic coordinates until required precision is obtained. After that the ions are moved according to the acting forces. Afterward, another self-consistent electronic loop is carried out and so on, until obtained accuracy is achieved.

Variational principle is very important for finding ground state and it applies (with slight differences) both for wave function approach (HF and post-HF methods) and for electron density approach (DFT methods). It states that the computed energy is always greater or equal to the ground state energy. It means that every calculation step leading to a lower system energy is a step towards more precise ground state wave function (or electron density).

As complexity of computation increases with number of electrons included in the calculation, it is beneficial to use as fewer electrons as possible. It is long time known that chemical properties of atom are at most determined by its valence electrons, while direct influence of core electrons is negligible. It seems straightforward to substitute the core electrons by some potential that explicitly enters the calculation, represents well potential of all core electrons but also has modest computational demands. This potential is, in contrast to the standard potential, energy-dependent, therefore it is called pseudopotential. It should fulfil following criterion – it should well describe long-range interaction of the core, inside the core radius it should be as soft as possible to save computational resources, and outside of the core radius pseudo wave function should be nearly identical to the full wave function. Two main approaches exist, the first is norm-conserving (it is normalized), the second one is ultra-soft, it does not fulfil norm-conserving criterion but uses other tricks to represent the core well. Pseudopotentials are generated from all-electron calculation for isolated atom following cumbersome and demanding procedure.

1.4.2 Basics of density functional theory

DFT is younger theory that significantly reduces computation times in contrast to the classical Hartree-Fock (HF) and post-HF methods. In those methods during relaxation procedure, the wave function, which is function of $3N$ variables (N standing for number of electrons), is relaxed. Those calculations scale very quickly with system size and are extremely demanding or intractable for systems consisting of tenths of atoms. Another ancestor of DFT was Thomas-Fermi theory, which proposed relation between effective potential and electron density $n(r)$ in each point of examined space. The drawback of the method is its non-universality – it is usable just for systems with constant external potential (potential of nuclei is labelled as external, as was proposed in Born-Oppenheimer approximation), or with just negligible potential gradient. Also, relation between Thomas-

Fermi equation and many-body wave function is not clear. The connection was later described in Hohenberg-Kohn theorem, which is the basis of the DFT.

Hohenberg-Kohn theorem states that effective potential of system is uniquely described by the ground-state of density of interacting electrons in given external potential. They proved by contradiction that two different external potentials cannot lead to the same electron density. Moreover, if number of electrons (N) is preserved in the system, the full Hamiltonian is then determined and, therefore, all quantities derivable from it are also obtainable.

Energy of system in DFT is determined by the energy functional. The total energy functional is expressed as:

$$E_{tot} = \min_{n(r)} E\,[n] = \min_{n(r)}(T[n] + V_{ext}[n] + V_H[n] + E_{xc}[n]) \qquad (6)$$

where $T[n]$ is kinetic energy functional of non-interacting electrons (which is unfortunately not well known), $V_{ext}[n]$ is external potential functional, $V_H[n]$ is electrostatic potential functional (corresponding to the electrostatic interaction term in HF theory), $E_{xc}[n]$ is exchange-correlation functional that contains all many-body effects. The latter is the biggest drawback of the DFT, as its form is unknown, and it is probably impossible to analytically determine it. On the other hand, it is universal functional of electron density, independent on particular system.

In contrast to the HF and post-HF methods, relaxation should be much easier. Following variational principle, just electron density (function of three coordinates) would be relaxed, instead of wave function consisting of $3N$ variables (as mentioned above). This would lead to the orbital-free DFT approach, which is still rather developing than commonly used. Practically, now the variation of electron density is not as easy, as not-well-known form of $T[n]$ should play important role. It seems to be advantageous to express electron density as sum over single-particle states (using Born's representation of wave function):

$$n(r) = \sum_{i=1}^{N} |\psi_i(r)|^2 \qquad (7)$$

Therefore, for total energy minimization considering single particle states, Kohn and Sham were able to propose equations (that are similar to HF equations), which are today known as Kohn-Sham equations:

$$\left\{-\frac{\hbar}{2m}\nabla^2 + v_{ext}(r) + v_H(r) + v_{xc}(r)\right\}\psi_i(r) = \varepsilon_i\psi_i(r) \tag{8}$$

where the first term in curly brackets stands for kinetic energy and the other terms together define effective one-electron potential acting on the electrons. Considering that exchange-correlation potential ($v_{xc}(r)$) can be expressed as

$$v_{xc}(r) = \frac{\delta E_{xc}[n]}{\delta n} \tag{9}$$

the total energy of ground state has form:

$$E = \sum_{i=1}^{N} \varepsilon_i + E_{xc}[n] - \int v_{xc}(r)n(r)d^3r - V_H + V_{nucl-nucl} \tag{10}$$

The equation differs from formulation of Hartree by just exchange-correlation terms, thus it is sometimes considered to be its formal extension, but, in contrast to Hartree and HF theory, the determined ground state should be exactly described. The accuracy of DFT is strongly dependent on precision of implementation of the exchange-correlation term. Unfortunately, as its form for general system is not exactly known, one has to use other approximations.

The exchange-correlation term is known and well-formulated for systems with constant electron density – homogenous electron gas. Local density approximation (LDA) aims to adjust this knowledge on examined systems with non-homogenous density. It assigns local exchange-correlation energy to every point in space as it was in homogenous electron gas with corresponding electron density. The total exchange-correlation energy is then sum of the local exchange-correlation energies. LDA fundamentally ignores the fact, that real exchange-correlation energy is non-local. Regardless of it, LDA predicts in many bulk systems very precise results. This was not still well described, but the commonly accepted explanation is that contradictory errors in terms of exchange and correlation eliminate one another. For systems in gas phase or containing surfaces, LDA usually predicts over-binding – the cohesive energies are much higher than obtained by experiment and predicted bond lengths are shorter than observed.

Significant improvement was achieved in the generalized gradient approximation (GGA). It uses local electron density (as LDA) for construction of local exchange-correlation energies but counts also with a gradient of the density. Together with adding general scaling properties and considering asymptotic behaviour of effective potentials, GGA predicts very precise

solutions for many systems and quickly overcame LDA. Most importantly for this work, GGA is significantly better than LDA for magnetic metallic systems. In GGA many different exchange-correlation functionals exist, for instance functional by Perdew and Wang (PW91) or Perdew, Burke and Ernzerhof (PBE). The choice of functional plays important role and can, in principle, lead to different results. Moreover, using of each functional is uncontrolled approximation and there is no systematic path to its improvement. This is not the only drawback of GGA (and DFT in general), it also fails in some specific cases, for instance in description of long-range and van der Waals interactions. Some of the problems were solved in *meta*-GGA approach (counts with higher orders of electron density gradient) and when using orbital functionals (the exchange-correlation functional depends on the particular orbital rather than on local electron density), but it resulted in much higher computational costs.

Spin-polarized DFT accounts for magnetism. In those calculations, the electron density is substituted by 2 x 2 Hermitian density matrix. Exchange-correlation GGA functionals must be (and the most popular are) adapted for this approach. If external magnetic field is collinear, every system can be reoriented to such way, that the external field is aligned with direction of its z-axis. In those cases the spin-up and spin-down components are treated nearly independently. Total magnetic moment (in Bohr magnetons) of supercell is then defined as difference between the count of spin-up and spin-down electrons. If external magnetic field is non-collinear, the spin-up and spin-down components cannot be treated separately, present Hamiltonian matrix is twice the size and calculations are much more demanding.

1.4.3 Bloch theorem, plane waves, k-points

For periodic systems the computation can be significantly simplified using famous Bloch theorem. It uses following derivation – many schemes of solving one-particle Schrödinger equation fulfil the criterion for periodic one-particle effective potential

$$v_{eff}(r) = v_{eff}(r + R) \tag{11}$$

where R is any Bravais lattice vector. One can thus assume that

$$\psi_i(r + R) = c_i(R)\psi_i(r) \tag{12}$$

where $c_i(R)$ is complex number with modulus equal to 1, it can be therefore expressed as

$$c_i(R) = e^{ikR} \tag{13}$$

where k is crystal-momentum and acts like quantum number. Considering above mentioned relations, the eigenfunction can be rewritten to form

$$\psi_k(r) = e^{ikR} u_k(r) \tag{14}$$

with u_k standing for periodic function that fulfils the following criterion

$$u_k(r) = u_k(r + R) \tag{15}$$

for all vectors R.

The basis set for periodic DFT is within plane waves, as this is computationally very efficient and allows easy change via Fast Fourier Transform (FFT) from a real-space representation (where the potential energy is diagonal), to momentum-space (where the kinetic energy is diagonal). Basis set consisting of atomic orbitals can thus be omitted – basis set of plane waves is used instead, as plane waves fulfil the criterion demanded by Bloch theorem. Expansion of any wave function entering the Kohn-Sham equations includes plane waves that vary just by the vector of reciprocal lattice. Eigenfunctions are then

$$\psi_k^G(r) = \frac{1}{\sqrt{V}} e^{i(k+G)r} \tag{16}$$

with G standing for reciprocal lattice vector and k lying inside the first Brillouin zone. The ground state energy is thereafter evaluated as an integral over the first Brillouin zone, the sum consists of all occupied energy bands. Evaluation of this integral would be much demanding, fortunately, it can be replaced by set of k-points that are inside the first Brillouin zone. This approximation is relatively accurate and, moreover, can be well controlled by the number of k-points. The reliability of results can be checked by increment of number of k-points which always leads to more precise solution. The above described principle is implemented in the way that Kohn-Sham equations are performed for each k-point. After that the energies of each occupied state of every k-point are summed to the total energy. After the self-consistent step, Fourier transformation is used to determine the electronic density in real space.

This whole approach could look unprofitable, as it adds many new steps to the calculations. In real, it significantly simplifies the whole solution, as it enables direct evaluation of the kinetic energy of electrons (through the momentum space), while potential energy is evaluated in real space. Kinetic energy also provides convenient control over the plane wave basis set – in these DFT calculations just one parameter (cutoff energy), is used. It directly determines the size of basis set, as only waves with smaller kinetic energy are

included in the calculation. The drawback of this approach is the demand of periodicity of examined system in all three directions. It also needs periodic boundary conditions of supercell that can introduce new imprecision.

Pseudopotentials here play very important role similarly as in the HF approach. Their softness has even greater impact, as it directly influences the number of plane waves that are needed for proper description of the system. However, interaction between core and valence electrons in some atoms is remarkable and they need all-electron approach for accurate solution. Probably the most successful method to consider all electrons with efficiency of ultra-soft pseudopotentials is the projected augmented wave (PAW) method. Its ancestor is the method of augmented plane waves (APW) proposed by Slater. He suggested to use different basis sets to expand the wave function inside and outside the core region. This basis sets consist of APW - they are augmented in the core region by spherical harmonics and radial function terms. Although this solution is in principle exact, the calculations are rather expensive and cannot comprehend whole energy spectrum. Following method of linearized augmented plane waves (LAPW) presented further conditions that introduce small errors, but basis wave functions are no more energy dependent and radial functions need to be determined just once during the calculation. The calculations are much simpler, however, new problem with determination of forces acting on atoms arose. Hellmann-Feynman forces are not sufficient for these basis sets and additional Pulay forces must be considered. LAPW gives probably the most precise results among all DFT methods. PAW method determines partial wave expansions by overlap with localized projector functions. This method has many properties with ultra-soft pseudopotential method in common, and it combines its efficiency with the precision of LAPW.

In PAW method the local magnetic moments located on each atom in system are evaluated using integration of its local DOS. It is created by projection of the plane waves of all occupied eigenstates onto spherical waves inside the atomic radius. PAW has its own implementation[38] of non-collinear magnetism. The wave function (Ψ_n^a) is product of

$$|\Psi_n^a\rangle = |\widetilde{\Psi}_n^a\rangle + \sum_i \left(|\Phi_i\rangle - |\widetilde{\Phi}_i\rangle\right) \langle \widetilde{p}_i | \widetilde{\Psi}_n^a \rangle \qquad (17)$$

where terms are pseudo-wave function ($\widetilde{\Psi}_n^a$), partial waves (Φ_i), pseudo partial waves ($\widetilde{\Phi}_i$), projector functions ($\widetilde{p}_i$), i represents all the variables (quantum numbers l and m and number k which points to the reference energy ε_{kl}) within core region. Pseudo-wave function is

constructed from 2*N* eigenspinors, where *N* stands for the number of eigenvalues. Partial waves are constructed with respect to the nonmagnetic atom, pseudo partial waves are equal to partial waves outside the core radius but are different inside this radius. Pseudo-wave functions can be used for direct evaluation of pseudo density matrix $\left(\widetilde{n^{\alpha\beta}}(r)\right)$, the on-site matrices $\left({}^{1}n^{\alpha\beta}(r)\right)$ and $\left(\widetilde{{}^{1}n^{\alpha\beta}}(r)\right)$ are calculated (from partial waves and pseudo partial waves, resp.) on support grid covering the space inside the core radius. Total density matrix is then evaluated as:

$$n^{\alpha\beta}(r) = \widetilde{n^{\alpha\beta}}(r) + {}^{1}n^{\alpha\beta}(r) - \widetilde{{}^{1}n^{\alpha\beta}}(r) \tag{18}$$

2 Computational details

2.1 Computational Parameters, Structure of Basic Cell

All calculations were performed using Vienna *ab-initio* simulating package (VASP)[39–41] that implements projected augmented wave (PAW) method[42] to describe electron-ion interaction. The functional of Perdew, Burke and Ernzerhof[43] (PBE) was used for evaluation of electronic exchange and correlation. It is a derivation of Generalized gradient approximation (GGA) that uses as parameters just internal constants. All executed calculations were spin-polarized, the symmetry was switched-off. The plane wave basis set contained waves with kinetic energy smaller than 400 eV. For electronic optimization the blocked Davidson algorithm was chosen.

The criterion for electronic convergence was 10^{-6} eV and forces acting on every atom had to be smaller than 0.01 eV/Å, the *k*-point mesh was Γ-centred and consisted of 12 x 12 x 1 *k*-points. During all steps the Gaussian smearing of width 0.02 eV for partial occupancies of orbitals was used. In first 2 steps the conjugate-gradient algorithm for ionic movement was used, in the next 2 steps RMM-DIIS (quasi-Newton) algorithm was used instead. In the static calculations performed after successful ionic relaxation, the tetrahedron method with Blöchel corrections with the same width of smearing was used as well as the same *k*-point mesh.

A single graphene sheet with single vacancy and with double vacancy was considered as well as its analogues with vacancies decorated by pyridinic nitrogen atoms. The latter systems are, respectively, termed single vacancy graphene with pyridinic nitrogen atoms and double vacancy graphene with pyridinic nitrogen atoms. Their structures are shown in Fig. 2.

In this work, graphene was represented by a supercell containing 50 C atoms. That should be large enough to avoid interaction between two vacancies, but also small enough to save computational times. The vertical distance between two graphene sheets (vacuum layer) was 14 Å to avoid the interaction between two graphene sheets due to the periodic boundary conditions.

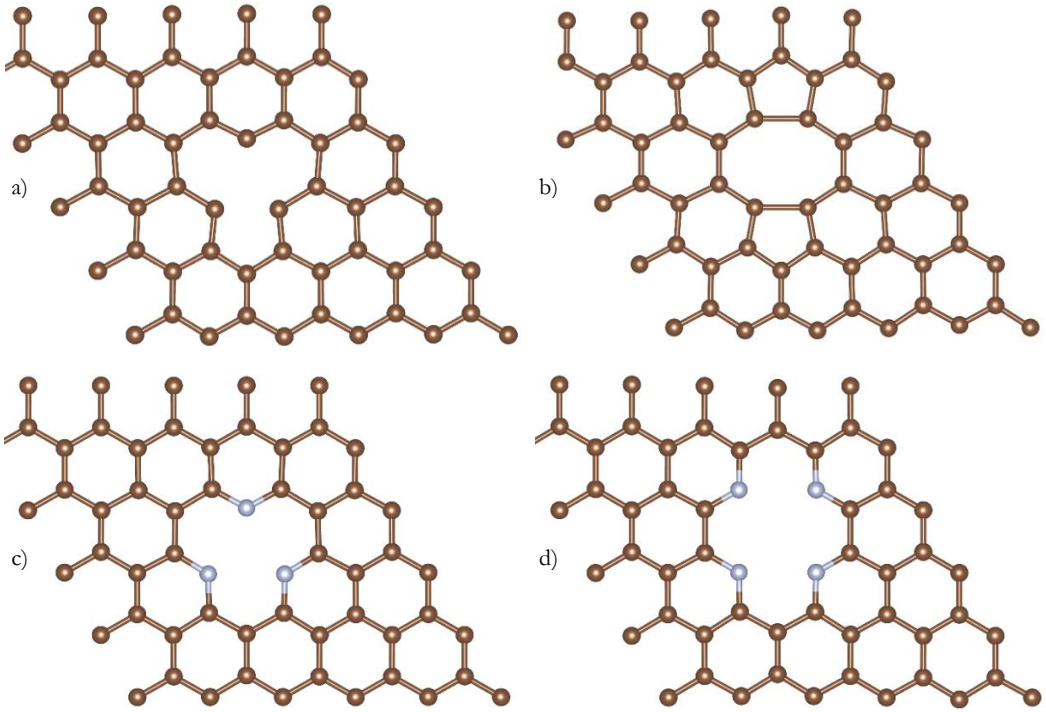

Fig. 2: Relaxed structures of a) SVG, b) DVG, c) SVNG, d) DVNG

2.2 Ionic Relaxation, Structures and Adsorption Energies

In the first place it was necessary to obtain ground state structures. Graphene sheet with the lattice constant of 2.47 Å and consisting of 50 atoms was taken, one (SVG, SVNG) or two carbon atoms (DVG, DVNG) were removed. Total formation energy (E_C, creation, so it is not misled with Fermi energy) is estimated as:

$$E_c = E_{VG} - E_{gra} + n \cdot \mu_C \tag{19}$$

where n is the number of removed C atoms, E_{VG} is total energy of relaxed defective system and E_{gra} is total energy of a perfect graphene system. Chemical potential of carbon atom (μ_C) is estimated as total energy of graphene per one C atom. In the case of SVNG and DVNG particular carbon atoms were substituted by nitrogen atoms. Those structures were relaxed as mentioned above. Their formation energy is evaluated with respect to the existing defective graphene systems:

$$E_c = E_{VNG} - E_{VG} + n \cdot \mu_C - n \cdot \mu_N \quad (20)$$

where chemical potential of nitrogen atom (μ_N) was estimated as a half of the total energy of dinitrogen molecule. After that single metal atoms (Fe, Co, Ni, Ru, Rh, Pd, Os, Ir, Pt) were initially placed 2.1 Å directly above the centre of the vacancy and the entire system was relaxed again. The structures were characterized by distance between adatom and its neighbours (d_{an}), vertical distance between adatom and its neighbour atoms (d_{van}), vertical distance between adatom and graphene sheet (uninfluenced graphene atoms) (d_{vag}) and graphene buckling amplitude (d_{ba}) defined as:

$$d_{ba} = d_{vag} - d_{van} \quad (21)$$

Stability of the adatom bonding to the defective graphene is quantified by the adsorption energy (E_{ads}) defined as:

$$E_{ads} = E_{vg+ada} - (E_{vg} + E_{ada}) \quad (22)$$

where E_{vg+ada} is ground state energy of system containing both vacancy graphene and adatom, E_{vg} of just vacancy graphene and E_{ada} of single adatom in vacuum. In this convention, the lower adsorption energy is, the more stable bond can be expected. In VASP it is recommended to perform static calculations (parameters mentioned above) to obtain the most accurate system ground state energies. In the case of free metal atoms in vacuum, the width of smearing was in some cases lowered to achieve integer population of energy levels in every atom.

2.3 Electronic Properties, Magnetism

DOS calculations were performed as part of the static calculations. The energy grid for evaluating DOS was set to be soft (consisting of 2800 energy levels). Results were processed using VSTS tool. All DOS plots were then created in Microsoft Excel. Fermi energy is in all plots shifted to 0.

Scalar-relativistic (SR) calculations provide magnetic moment of adatom, sum of local magnetic moments of all atoms forming defective graphene and total magnetic moment of the unit cell for all considered systems. Relativistic calculations including SOC were executed on all systems with non-zero magnetic moments obtained by SR calculations. MAE is defined as:

$$MAE = min(E_x, E_y) - E_z\,, \quad (23)$$

where E_x, E_y and E_z are total energies of systems with different initial orientation of magnetization – x and y correspond to the orientation within the graphene layer (parallel to graphene), z – perpendicular to it. In this convention, the positive value corresponds to the perpendicular easy axis. MAE determines the height of the barrier between easy and hard magnetization directions. The higher it is, the more stable information storage can be expected, because it resists higher temperatures better. Relativistic calculations were performed on relaxed systems. Atom coordinates were kept fixed, one self-consistent electronic loop was executed.

Bader charge analysis provides possibilities how to determine partial charge located on every atom in the system. Charge of the adatom could be important for properties of SAHC as localized charge could attract specific parts of molecules that should undergo the catalysed reaction and modify the catalyst's selectivity. Moreover, higher charge located on adatom could correlate with stronger binding. As Bader shown, local maxima of electron density are located at nuclei, further from nuclei the density vanishes. Nuclei is said to create around itself so called basin. In the basin all charge density gradient paths head towards the nuclei. One can then interpret the basin as atom.[44,45] Bader charge analysis was added to VASP owing to the Henkelman group[46]. Charge on every atom (Q) was evaluated as:

$$Q = N_{val} - N_{Bader} \tag{24}$$

where N_{val} is number of valence electrons in free atom, N_{Bader} is computed number of (valence) electrons in the atom that is in the system. In this convention, the charge corresponds to the ionic charge known from classical chemistry.

Charge density difference analysis is together with projected DOS (PDOS) and Bader charge analysis a powerful tool to research the bonding mechanism of the adatom. For this analysis it was necessary to run specific calculations. The supercell of fully relaxed system was divided to two new supercells with the same size. The first one included just the adatom, the second one just the defective graphene. The atoms were kept at the corresponding coordinates of the original supercell. Static calculations were then performed. The charge density difference was calculated using following equation:

$$Q = Q_{system} - (Q_{adatom} + Q_{defective\ graphene}) \tag{25}$$

where Q represents final charge difference, other Qs are charge densities of mentioned supercell. Positive value means that charge density in that point increased after the bonding of the adatom. From this grid isosurface covering significant positive charge region and

isosurface covering significant negative charge region were plotted in VESTA. Atomic positions were also included in this plot.

2.4 Preferred Adsorption Sites

TM atoms can adsorb at pristine graphene[47]. Each of elements prefers different position within graphene lattice[47]. The high-symmetry positions are called hollow (H, above the hexagon), bridge (B, above bond between 2 atoms) and top (T, above one carbon atom) as shown in Fig. 3. Local minima along the defective graphene (other than the position inside the vacancy) were also searched in this work and then their adsorption energy was compared with the adsorption energy in the vacancy to evaluate their significance. If the difference between the energies was low, the adatoms would not prefer to anchor to a vacancy and would rather stay elsewhere.

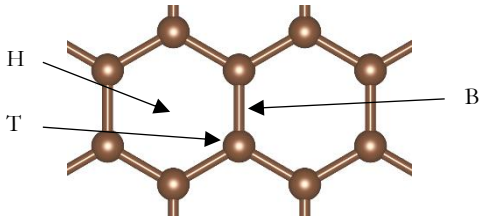

Fig. 3: Schemes of high-symmetry positions on graphene: hollow (H), bridge (B) and top (T).

Adatoms were placed in different initial positions (shown in Fig. 4), always 2.1 Å above graphene sheet. During relaxations all coordinates of all atoms were allowed to optimize. After each step, final positions of the adatoms were checked – if adatom in two different systems had very close final position (difference smaller than 0.13 Å), only one of these systems was taken to the next step because it significantly saved computational resources. Final positions after complete ionic relaxation were recorded. For these systems static calculations were also performed, so adsorption energies in these systems could be reliably compared with adsorption energy in the defect.

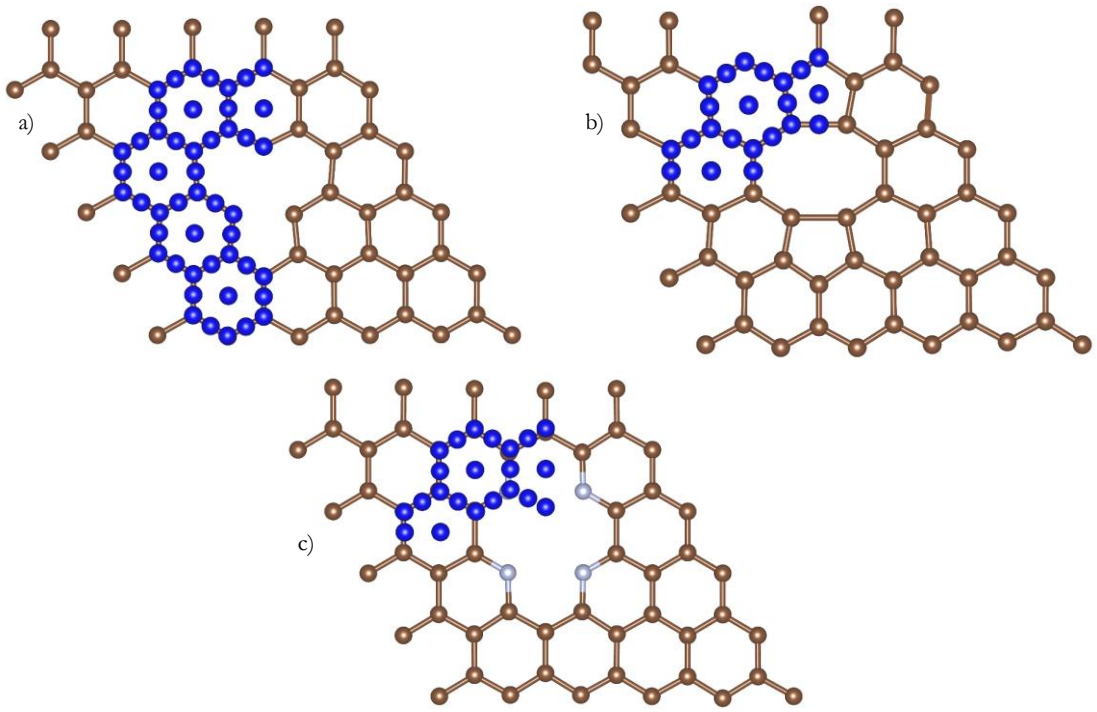

Fig. 4: Schemes of initial positions (marked by dark-blue dots) of adatoms: a) SVG, b) DVG and c) DVNG

3 Results and Discussion

3.1 Pristine defective graphene

As reference, relaxed vacancy graphene systems without adatom are examined. Structures were relaxed as described above. In SVG the newly created σ bond from two dangling bonds is 2.11 Å long, the distance between concerned atoms and the atom with dangling bond is 2.58 Å. The former length is slightly longer (+ 0.1 Å) than commonly accepted value.[23] Contrary to the literature[23], adatom with dangling bond is after relaxation placed in the graphene plane. System with initial position of C atom (with dangling bond) above the graphene plane was also considered – mentioned atom was shifted after relaxation 0.29 Å above the graphene plane, but this geometry was energetically unfavourable by ~ 30 meV. In-plane configuration is therefore considered to be the ground state. Formation energy is 7.73 eV, which is similar to the commonly reported results.[23] DOS of SVG is shown in Fig. 5a, it is in good agreement with Ref. [48]. Localized states are presented at E_F, spin channels are non-symmetric, and therefore the system is magnetic. Calculated value of magnetic moment (1.71 μ_B) is within wide range (1 – 2 μ_B) reported by other papers[23].

In DVG the new σ bonds have length of 1.83 Å, in reasonable agreement with Dai *et al.*[32] (1.78 Å). The distance between these bonds is 3.06 Å, it is in perfect agreement with Ref. [32].

Formation energy is 8.06 eV, in good agreement with reports by references[23] (~ 8 eV), but significantly lower than observed by Dai *et al.*[32] (9.00 eV). Since they used similar method and computational parameters, the reason for this discrepancy is unclear. DOS of DVG is shown in Fig. 5b, it is in reasonable agreement with Ref. [32]. DOS is symmetric and therefore DVG is nonmagnetic, which is in agreement with Ref. [32].

N atoms in SVNG are after relaxation (from in-plane configuration) slightly placed out of plane – one above (0.18 Å), one bellow (0.18 Å) and one in graphene plane. Average bond length C-N is 1.34 Å, similar to the observation of Fujimoto and Saito[33] (1.33 Å). Average distance between N atoms is 2.62 Å. Formation energy from existing SVG is -4.26 eV, in good agreement with Hou *et al.*[34] Magnetic moment of the system is 0.84 μ_B, close to the Ref. [33] (0.89 μ_B). DOS of SVNG with exchange-splitting of ~ 0.25 eV is shown in Fig. 5c.

In DVNG the N atoms form rectangle with sides long 2.62 Å and 2.83 Å similar to results by Choi *et al.*[49] (2.58 Å and 2.77 Å) and Hou *et al.*[34] (2.64 Å of the shorter one). Average distance C-N is 1.34 Å, which is very close to the value of Fujimoto and Saito[33] (1.32 - 1.33 Å). The formation energy from existing DVG is -4.24 eV, significantly lower value was obtained by Hou *et al.*[34] (- 3.6 eV). The possible reason for this discrepancy is

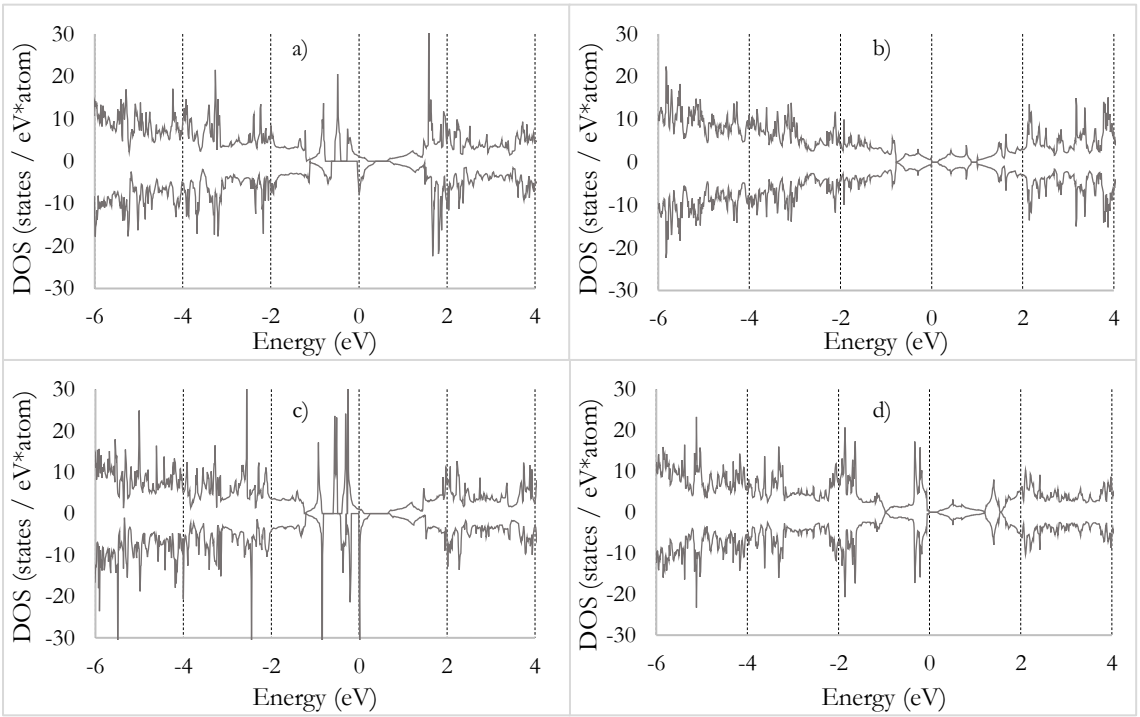

Fig. 5: DOS of pristine defective graphene: a) SVG, b) DVG, c) SVNG, d) DVNG.

different total energy of the DVG system – they evaluated formation energy of DVG to be 7.44 eV (the same discrepancy of ~ 0.63 eV). System has zero magnetic moment, similarly as in Ref. [33], and accordingly symmetric spin-up and -down DOS, which is shown in Fig. 5d.

3.2 Structures and Adsorption Energies

Tab. 1 lists adsorption energies and vertical distances (adatom – average graphene π-coordinate) together with values from available reference. Average bond lengths (adatom – neighbour), vertical distances (adatom – neighbour) and graphene distortion are shown in Tab. A1, A2 and A3 respectively. All the obtained quantities are represented in Fig. 6. For clarity the adatoms are divided to 3 groups – Fe group (Fe, Co, Ni), Ru group (Ru, Rh, Pd), Os group (Os, Ir, Pt).

PBE functional was used both in this work and also in all cited references. The obtained results are compared with literature in Tab. 1, where also the computational methods are listed – VASP with plane wave and PAW method, QUANTUM-ESPRESSO with plane-wave approach and pseudopotentials or DMol^3 with double numerical plus polarization basis set and semicore pseudopotentials. In the case of adsorption energy, 36 of 52 cited results are within deviation of ± 5 %, 43 are in agreement within ± 10 %. 5 of the result out of ± 10 % agreement were obtained using DMol^3 package, the remaining 4 were calculated using VASP package. The agreement is, at first sight, worse in the case of adsorption distances. The origins are mainly in the different criterion of adsorption distance evaluation, variant size of supercell (bigger supercell can lead to more significant buckling amplitude) or distinct initial positions before relaxation (embedding adatom to the graphene plane in the case of DVG and DVNG can lead to its stay in the graphene plane due to the reflection symmetry). If bond lengths were presented, they were often very close to those obtained in this work.

Among 3 groups of elements, the trends in adsorption energies are similar for SVG and SVNG, and DVG and DVNG. Stronger binding was found for SVG than for SVNG (of about 2.5 eV), which is among all the systems weakest. Conversely, adatoms bind more strongly to DVNG than DVG. In DVG and DVNG, exceptions are Ru and Os, while similar binding energy was found for Ir. Trend in DVNG can be explained according to the covalent

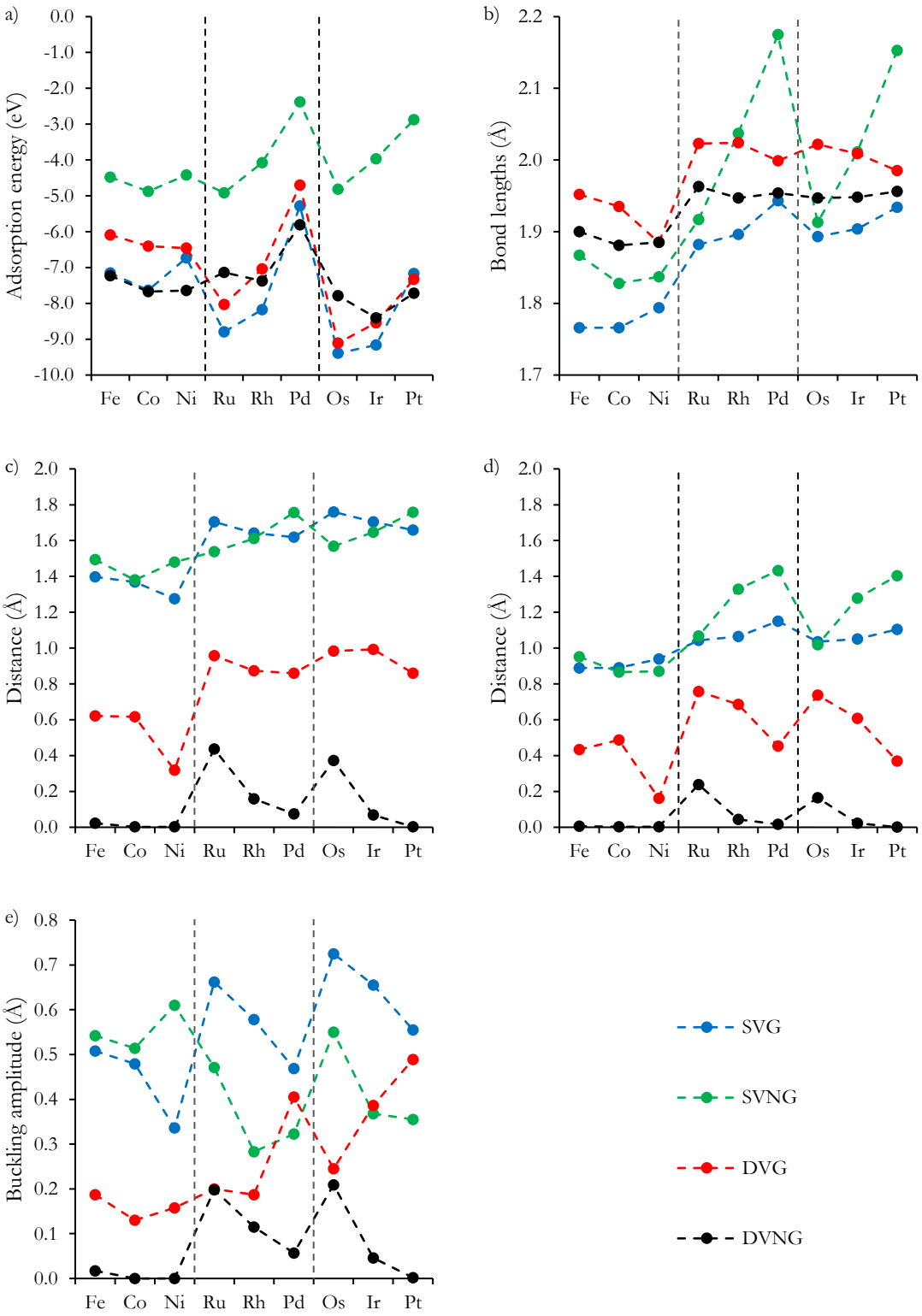

Fig. 6: Adsorption energy and geometric properties of relaxed defective graphene systems with adsorbed adatoms. a) adsorption energy, b) average bond lengths (adatom – neighbour), c) vertical distance (adatom – average graphene z-coordinate), d) vertical distance (adatom – average neighbour z-coordinate), e) graphene buckling amplitude.

Tab. 1: Adsorption energies and adatom adsorption distances (adatom – average graphene z-coordinate) in defective graphene systems – present work (Pres.) compared with references (Ref.): Gao *et al.*[50] (VASP), Krasheninnikov *et al.*[51] (VASP), Raji *et al.*[52] (QUANTUM-ESPRESSO), Santos *et al.*[53] (VASP), Sun *et al.*[54] (VASP), Guo *et al.*[55] (VASP), Ambrusi *et al.*[56] (VASP), Zhou *et al.*[57] (DMol^3), Ma *et al.*[58], (VASP), Sun *et al.*[59] (VASP), Han *et al.*[60] (VASP), Fampiou *et al.*[61] (VASP), Kattel *et al.*[62] (VASP), Zhang *et al.*[63] (DMol^3), Yang *et al.*[64] (DMol^3), Zhou *et al.*[65] (DMol^3), Zhao and Wu[66] (DMol^3), Rangel and Sansores[67] (QUANTUM-ESPRESSO), Rafique *et al.*[68] (VASP). Rafique *et al.*[69] (VASP), Ge *et al.*[70] (VASP).

		Adsorption energy (eV)				Adsorption distance (Å)			
		SVG	SVNG	DVG	DVNG	SVG	SVNG	DVG	DVNG
Fe	Pres.	- 7.150	- 4.479	- 6.095	- 7.228	1.397	1.493	0.621	0.023
	Ref.	- 7.14 [50]	- 4.41 [50]	- 6.12 [50]	-7.14 [50]	1.345 [50]	1.230 [50]	0.660 [50]	0.053 [50]
		- 7.3 [51]	- 4.48 [62]	- 6.2 [51]	- 7.07 [62]	1.35 [51]	1.33 [62]	0.6 [51]	0 [62]
Co	Pres.	- 7.635	- 4.875	- 6.406	- 7.674	1.369	1.380	0.617	0.002
	Ref.	- 7.6 [51]	- 4.90 [62]	- 6.4 [51]	- 7.54 [62]	1.45 [51]	1.25 [62]	0.55 [51]	
		- 7.51 [52]	- 4.84 [63]	- 6.1 [52]	- 7.6 [64]	1.42 [52]		0.68 [52]	
Ni	Pres.	- 6.734	- 4.419	- 6.461	- 7.644	1.275	1.480	0.319	0.002
	Ref.	- 6.9 [51]	- 3.7 [64]	- 6.8 [51]	- 7.8 [64]	1.2 [51]	0.94 [65]	0.25 [51]	
		- 7.0 [53]	- 5.09 [65]			1.21 [53]			
Ru	Pres.	- 8.792	- 4.915	- 8.030	- 7.141	1.705	1.538	0.958	0.436
	Ref.	- 9.15 [54]		- 5.42 [55]					
		- 8.57 [55]							
Rh	Pres.	- 8.179	- 4.073	- 7.039	- 7.375	1.642	1.612	0.873	0.159
	Ref.	- 8.37 [56]	- 4.33 [66]	- 7.44 [56]		1.50 [56]	1.422 [66]	0.84 [56]	
		- 8.5 [54]							
Pd	Pres.	- 5.283	- 2.383	- 4.705	- 5.808	1.619	1.756	0.859	0.074
	Ref.	- 5.10 [57]	- 4.44 [66]	- 4.23 [57]		1.624 [57]	1.614 [66]	0.866 [57]	
		- 5.37 [58]	- 2.46 [67]	- 4.64 [58]		1.52 [58]	1.61 [67]	0.61 [58]	
Os	Pres.	- 9.394	- 4.818	- 9.110	- 7.784	1.760	1.569	0.983	0.373
	Ref.	- 9.8 [59]	- 5.46 [68]	- 8.57 [69]	- 8.49 [68]		1.52 [68]	0 [69]	0 [68]
Ir	Pres.	- 9.165	- 3.970	- 8.541	- 8.402	1.705	1.646	0.993	0.068
	Ref.	- 9.7 [59]	- 4.76 [68]	- 8.71 [69]	- 8.61 [68]		1.68 [68]	0 [69]	0 [68]
		- 9.80 [60]		- 8.64 [70]				0.597 [70]	
Pt	Pres.	- 7.166	- 2.874	- 7.328	- 7.717	1.659	1.758	0.859	0.003
	Ref.	- 7.0 [51]	- 2.87 [68]	- 7.1 [51]	- 7.74 [68]	1.8 [51]	1.66 [68]	0.7 [51]	0 [68]
		- 7.45 [61]	- 3.31 [66]	- 6.12 [61]		1.12 [61]	1.600 [66]	0.31 [61]	

radii of adatoms. Covalent radii descend in all groups. Bigger atoms (Ru and Os in particular) cannot fit to the vacancy of DVNG and graphene is thus distorted, and the binding is weakened.

Average bond lengths in SVG are the shortest from all systems, they show systematic tendency to increase in groups, and they are shortest for Fe group. Bond lengths in Ru and Os groups are very similar. The trend in SVNG is similar, but the increment in Ru and Os groups is much more pronounced (from 1.9 to 2.2 Å). DVG is the only defective graphene system, where bond lengths shorten in each group. The shortening is most pronounced in the Fe group. In DVNG the change in bond lengths in groups is (in comparison with other defective graphene systems) negligible, there is just one shift between Fe and Ru group of ~ 0.5 Å to longer bonds.

Vertical distances (adatom – neighbour, d_{van}) follow similar trend as bond lengths. Small differences are observed in SVG, where total deviation is smaller than 0.3 Å. In SVNG the increment in groups is more significant (total deviation 0.5 Å). This distance is globally shorter in DVG and shortest in DVNG, it, conversely than in SVG and SVNG, even shortens in groups. In DVG the total deviation of 0.6 Å is the biggest among all the systems. In DVNG the adatoms are placed in the graphene plane or slightly above the neighbours (d_{van} smaller than 0.24 Å).

In SVG, vertical distance (adatom – average graphene z-coordinate, d_{vag}) shows completely opposite tendency than d_{van} – it descends in groups, moreover, with more significant magnitude. This gives rise to significant graphene buckling, in Fe group slightly lower than in SVNG systems, but the highest in Ru and Os groups, which have also similar values. Buckling amplitude follows the same trend as d_{vag}, but the difference in groups is even more pronounced. In SVNG systems, the d_{vag} in Ru and Os groups slightly increases, graphene buckling amplitude does not follow any systematic trend. In DVG the d_{vag} with small deviations follow the same trend as d_{van}, graphene buckling amplitude has no observable tendency. In DVNG systems, d_{vag} strictly follows d_{van} but with more pronounced magnitude, which gives rise to the same trends in buckling amplitude.

At first, just qualitative analysis of trends observed in graphs is discussed, in next paragraph the correlation between obtained values is mathematically summarized. In SVG, absolute value of adsorption energy proportionally correlates with d_{vag} and buckling amplitude and inverse-proportionally correlates with bond lengths and d_{van}. In SVNG, absolute value

of adsorption energy inverse-proportionally correlates with bond lengths, d_{van} and d_{vag}. In DVG, absolute value of adsorption energy inverse-proportionally correlates with bond lengths, d_{van} and d_{vag}. As adsorption energy in DVNG has minimum in middle of each group, just the inverse-proportional correlation between bond lengths and absolute value of adsorption energy is worth mentioning.

Global dependence of obtained values on the adsorption energy as well as on the order number of adatom (adatoms numbered from 1 to 9, starting from Fe = 1) is presented. It is advantageous to distinguish between global trends (already presented) and between trends in groups – for these purposes, correlation coefficient is calculated for each group and then the three resulting coefficients are averaged. If trends in groups are similar but no significant global trend is observed, this correlation coefficient has more pronounced value than the global one, see for instance the dependency of adsorption energies and bond lengths in SVG. All correlation coefficients are presented in the Tab. 2.

Tab. 2: Correlation coefficients between obtained values, for further explanation see the end of this subchapter. The abbreviations on the left-hand side stand for global correlation (GE) and average correlation (AE) with adsorption energy; global correlation (GN) and average correlation (AN) with order number of adatom. Top abbreviations stand for adsorption energy (AdE), bond lengths (BL), vertical distance (adatom – neighbour, VN), vertical distance (adatom – average graphene z-coordinate, VG) and buckling amplitude (BA).

		AdE	BL	VN	VG	BA
SVG	GE		-0.06	0.09	-0.50	-0.81
	AE		0.94	0.94	-0.80	-0.88
	GN	-0.22	0.88	0.81	0.77	0.50
	AN	0.77	0.93	0.92	-0.97	-0.98
SVNG	GE		0.91	0.83	0.87	-0.68
	AE		0.86	0.77	0.99	-0.22
	GN	0.55	0.74	0.74	0.82	-0.57
	AN	0.70	0.42	0.37	0.62	-0.32
DVG	GE		-0.46	-0.59	-0.52	-0.03
	AE		-0.39	-0.50	-0.37	0.90
	GN	-0.45	0.57	0.22	0.67	0.84
	AN	0.34	-0.93	-0.91	-0.88	0.44
DVNG	GE		0.18	0.03	0.05	0.07
	AE		0.52	0.28	0.23	0.17
	GN	-0.20	0.75	0.08	0.14	0.19
	AN	0.01	-0.13	-0.90	-0.92	-0.94

Values in Tab. 2 are rather diverse, from direct correlation (1) via no correlation (0) to inverse correlation (-1). In many cases, global correlation is remarkably different from average correlation in groups which points to the quantities that ascend (descend) in groups, but values in the next group are not higher (lower) than in the previous group. In SVG the values strongly correlate (with exception of GE), AE and AN point to the similar results. In SVNG GE and AE point to the stronger dependence than GN and AN but all the correlations are in good agreement. In DVG the most remarkable correlation is AN (with exception of BA), GE and AE are weaker and GN predicts opposite and weaker correlation than AN. In DVNG GE and AE are rather weak, bond lengths correlate well with GN. The most remarkably, VN, VG and BA correlate very well with AN, which could reflect the dependency of the adatom size.

3.3 Preferred Adsorption Sites

Preferred adsorption site analysis was performed for all adatoms at DVG and DVNG. Adatoms at graphene are rather mobile and in many cases, they shifted directly to the vacancy (as was assumed in all above mentioned systems). If they shifted to other local minima, the binding was remarkably weaker. Anchoring adatom to the vacancy is therefore favourable event. On the other hand, other calculations, taking into account more than single TM atom, would need to be performed to reveal whether this anchoring is strong enough to prevent the adatoms from clustering.

Ref. [71] showed that Ir-Co dimer in SVG and SVNG systems also shifts to the vacancy. Moreover, this behaviour was observed for dimer in both possible upright positions (Co atom closer and farther from graphene). For confirmation, Ir adatom at SVG was also examined in present work and its shift towards vacancy was also observed. We therefore humbly expect that adatoms could also move along SVG and SVNG graphene to anchor to the vacancy. Calculations confirming or rejecting this hypothesis will be performed soon.

3.4 Density of States, Magnetism, Bader Charges, Charge Density Difference

Comparison of values of charges located on adatom and total magnetic moment with available reference is shown in Tab. 3. Values of adatom magnetic moment, sum of magnetic moments of all atoms other than adatom and second biggest magnetic moment are shown in Tab. A4, A5 and A6 respectively. All obtained values are represented in Fig. 7. As in the previous subchapter, the adatoms are divided to 3 groups – Fe group (Fe, Co, Ni),

Ru group (Ru, Rh, Pd), Os group (Os, Ir, Pt). Bader charges, charge density difference and DOSs of all examined systems are shown in Appendix 2.

The same rules as mentioned in the subchapter 3.2 apply for description of methods of references – with one exception – Ref. [72] used revised PBE (RPBE) functional. Charge located on adatom seems to strongly depend on the used charge analysis (Bader or Mulliken method – results obtained by these methods are not comparable, but for some systems just the results predicted by Mulliken method were found, so they were left for illustration), therefore it is noted in Tab. 3 together with used computational method. Just 6 of 23 compared values are in agreement within ± 5 %, 7 of 23 agree within ± 10 %. Charges obtained by Mulliken method predict much lower charge transfer in 5 / 6 cases, on the other hand, Bader analysis performed by Refs. [72,73] suggests in all (except one) compared cases much more significant charge located on adatom. In comparison of total magnetic moments, 28 of 38 compared results agree with deviation of ± 5 %, 29 within ± 10 %. What is surprising – all the results with greater deviation were obtained by references using VASP, the most significant disagreement is with Refs. [68,69], which in DVG and DVNG systems initially placed the adatom directly to the graphene plane and their resulting geometries were different from final positions in this work.

Adatom always donates electrons to the graphene lattice (thus TM could be considered as *n*-type dopant). The amount of relocated charge descends in all groups. The highest charge transfer is observed in DVNG and then SVNG systems. This is due to the presence of nitrogen atoms which have higher value of electronegativity and thus attract electrons more than carbon atoms. Less remarkable charge transfer is presented in DVG and SVG systems.

Total magnetic moment in SVG follows interesting trend – its value for the first and third member of each group is zero, but it is ~ 1 μ_B for the second member. Very similar tendency can be also observed in the case of DVG systems with exception of Fe adatom – here the total magnetic moment is the highest of all observed (3.39 μ_B). The value of each second member also seems to decrease by ~ 0.1 μ_B. In SVNG the trend is similar – system with Fe adatom is again unsystematically very high, in addition, the third member of each group has value of 1 μ_B (Ni system even 1.57 μ_B) and the second member ~ 2 μ_B with descending trend

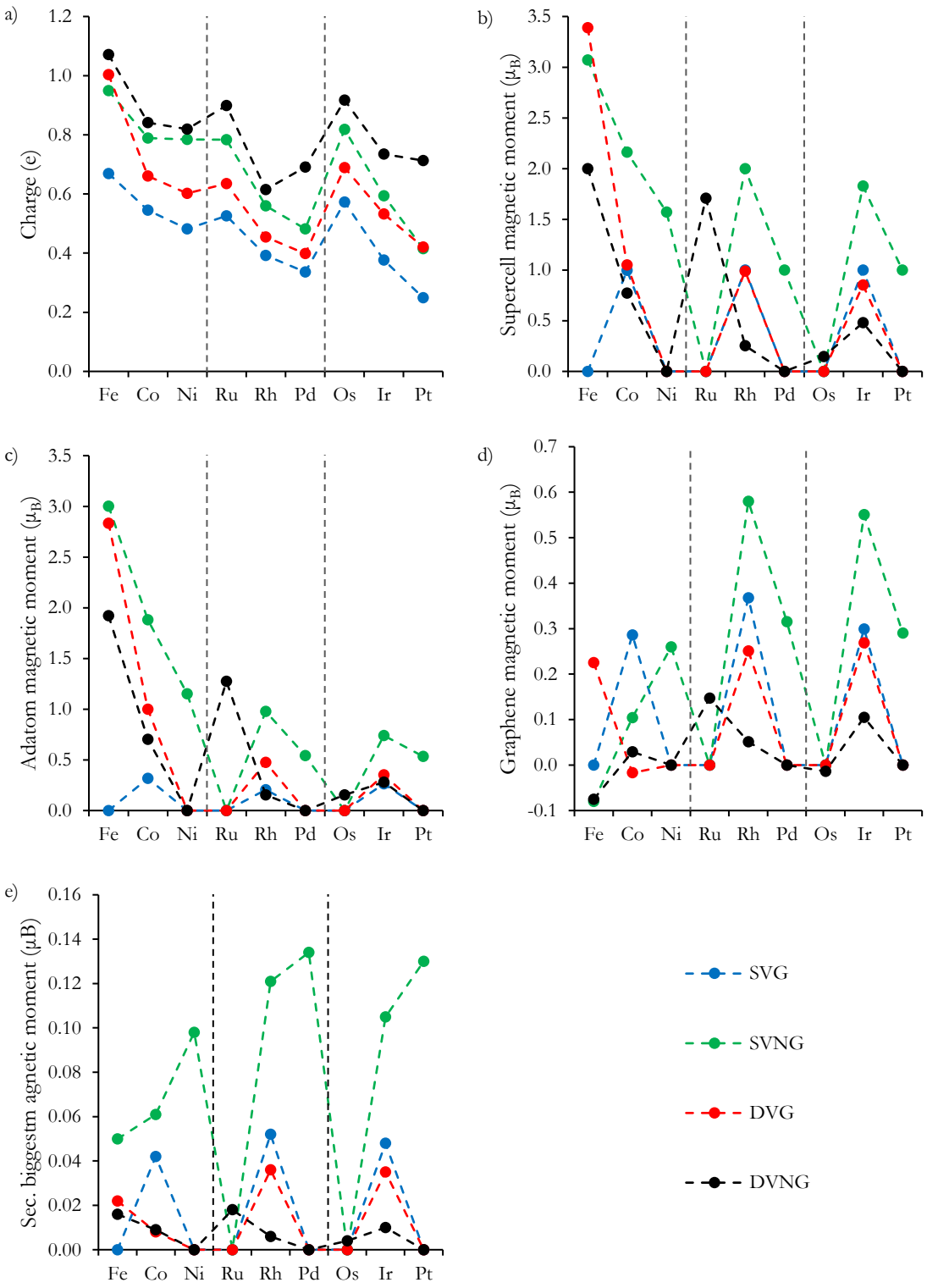

Fig. 7: Electronic and magnetic properties of relaxed defective graphene systems with adsorbed adatoms. a) charge located on adatom, b) total magnetic moment of supercell, c) local magnetic moment of adatom, d) sum of local magnetic moments of all atoms forming defective graphene, e) second biggest magnetic moment presented in system.

Tab. 3: Charge located on adatom and total magnetic moment in defective graphene systems – present work (Pres.) compared with references (Ref.). In case of reference to electronic charge, also method of its evaluation is mentioned. References: Gao *et al.*[50] (VASP, Bader), Krasheninnikov *et al.*[51] (VASP), Raji *et al.*[52] (QUANTUM-ESPRESSO), Santos *et al.*[53] (VASP), Sun *et al.*[54] (VASP), Guo *et al.*[55] (VASP, Bader), Ambrusi *et al.*[56] (VASP), Zhou *et al.*[57] (DMol^3, Mulliken), Sun *et al.*[59] (VASP), Kattel *et al.*[62] (VASP), Zhang *et al.*[63] (DMol^3, Mulliken), Zhao *et al.*[66] (DMol^3, Mulliken), Rangel *et al.*[67] (QUANTUM-ESPRESSO), Rafique *et al.*[68] (VASP), Rafique *et al.*[69] (VASP), Ge *et al.*[70] (VASP, not mentioned), Back *et al.*[72] (VASP, Bader), Tang *et al.*[73] (VASP, Bader), Fair *et al.*[74] (DMol^3).

		Charge located on adatom (e)				Total magnetic moment (μ_B)			
		SVG	SVNG	DVG	DVNG	SVG	SVNG	DVG	DVNG
Fe	Pres.	0.669	0.949	1.003	1.071	0.000	3.070	3.388	2.000
	Ref.	0.687 [50]	0.889 [50]	0.895 [50]	1.081 [50]	0 [51]	3.11 [62]	3.3 [51]	2.00 [62]
		1.07 [73]		1.33 [73]		0 [53]			
Co	Pres.	0.545	0.789	0.661	0.841	0.997	2.162	1.050	0.772
	Ref.	0.66 [72]	0.13 [63]			1 [51]	2.29 [62]	1.4 [51]	1.00 [62]
						1.00 [52]		1.08 [52]	
Ni	Pres.	0.482	0.784	0.602	0.819	0.000	1.570	0.000	0.000
	Ref.			0.75 [72]		0 [51]		0 [51]	
						0 [53]			
Ru	Pres.	0.526	0.783	0.635	0.899	0.000	0.000	0.000	1.708
	Ref.	0.54 [55]		0.64 [55]		0 [54]			
				1.10 [72]					
Rh	Pres.	0.392	0.560	0.454	0.615	1.000	2.000	0.988	0.253
	Ref.	0.58 [72]	0.30 [66]			0.965 [54]		0.76 [56]	
						0 [56]			
Pd	Pres.	0.336	0.482	0.398	0.691	0.000	1.000	0.000	0.000
	Ref.	0.147 [57]	0.35 [66]	0.398 [57]		0 [57]	1 [67]	0 [57]	
				0.63 [72]		0 [54]		0 [74]	
Os	Pres.	0.573	0.818	0.689	0.917	0.000	0.000	0.000	0.146
	Ref.			0.30 [72]		0 [59]	0.00 [68]	1.5 [69]	0.00 [68]
Ir	Pres.	0.376	0.594	0.532	0.735	1.000	1.827	0.852	0.480
	Ref.			0.556 [70]		0.99 [59]	1.30 [68]	0.838 [70]	0.75 [68]
				0.95 [72]				0.217 [69]	
Pt	Pres.	0.249	0.415	0.420	0.713	0.000	1.000	0.000	0.000
	Ref.		0.21 [66]	0.79 [72]		0 [51]	1.00 [68]	0 [51]	0.00 [68]
						0 [59]		0.00 [69]	

of ~ 0.17 μ_B. In DVNG the tendency seems to be descending within each group with exception of system with Os adatom that has very modest value of 0.14 μ_B which is lower than in the case of corresponding Ir system. Trends of adatom magnetic moments are similar.

Presence of adatom induces magnetism also in the other parts of defective graphene which is remarkable mostly in the SVG and SVNG systems, while it is very modest in DVNG systems. Generally, it seems to follow the trend of magnetic moment presented on adatom with exception in Fe and Co systems where the situation is completely different. Analysis of magnetic moments presented on each atom showed no significant values. They are represented as the second biggest magnetic moment. Their trend is also analogous with the only exception in the third members of each group in SVNG – here the magnetic moments (located on N atoms) are the highest observed. Correlation between all above mentioned properties and adsorption energy (or adatom number) is presented in Tab. 4.

Tab. 4: Correlation coefficients between obtained values, for further explanation see the end of subchapter 3.2. The abbreviations on the left-hand side stand for global correlation (GE) and average correlation (AE) with adsorption energy; global correlation (GN) and average correlation (AN) with order number of adatom. Top abbreviations stand for charge located on adatom (CHG), total magnetic moment (TM), adatom magnetic moment (AM), sum of magnetic moments of all defective graphene atoms (GM) and second biggest magnetic moment presented in the system (SM).

		CHG	TM	AM	GM	SM
SVG	GE	-0.27	-0.35	-0.32	-0.34	-0.36
	AE	-0.66	-0.55	-0.55	-0.55	-0.55
	GN	-0.76	0.00	-0.05	-0.02	0.03
	AN	-0.98	0.00	0.00	0.00	0.00
SVNG	GE	-0.84	-0.03	-0.20	-0.08	0.80
	AE	-0.51	0.27	0.34	0.32	0.71
	GN	-0.75	-0.52	-0.72	-0.61	0.34
	AN	-0.95	0.02	0.09	0.06	0.93
DVG	GE	-0.06	0.24	0.29	0.26	-0.13
	AE	-0.27	0.18	0.18	0.18	0.18
	GN	-0.69	-0.58	-0.65	-0.61	-0.02
	AN	-0.96	-0.33	-0.33	-0.33	-0.33
DVNG	GE	-0.09	0.03	0.06	0.04	-0.14
	AE	0.40	-0.19	-0.15	-0.19	-0.27
	GN	-0.58	-0.62	-0.67	-0.64	-0.48
	AN	-0.84	-0.74	-0.82	-0.76	-0.79

Correlation in this group is better to divide to two groups – CHG and magnetism. In CHG the correlation with GE and AE is relatively small, more pronounced dependency can be seen in GN and even more in AN, which could reflect the electronegativity of the adatom.

In case of magnetism, SVG shows just weak inverse correlation with AE. Most remarkable dependency in SVNG systems can be seen in SM (in this case the second biggest magnetic moment is always located on neighbouring N atoms). It is interesting because these systems also show significant dependency of bond lengths and vertical distances on the atomic numbers (see end of subchapter 3.2) – long vertical distances thus induce magnetic moments on the neighbouring N atoms. In DVG the most significant dependency can be seen in GN with TM, AM and GM. In DVNG the inverse correlation between GN and AN, and TM, AM and GM is remarkable. DVNG is (from SM point of view) completely opposite case than SVNG, there is inverse dependency of SM, similarly as of vertical distances (see end of subchapter 3.2), on the atomic numbers – it supports the hypothesis that magnetic moments induced on N adatoms correlate with vertical distances.

3.5 Magnetic anisotropy energy

SOC calculations for MAE evaluation were performed on all systems with non-zero magnetic moment from SR calculations. Calculated values are shown in Tab. A7 and in Fig. 8. Differences in spin and orbital magnetic moments of adatom between in-plane and perpendicular orientation of magnetization are shown in Tab. A8 and A9, resp. Value of MAE correlates with differences in spin and orbital moments with coefficients 0.61 and 0.55 resp., *i.e.* increment in magnetic moments in perpendicular orientation of magnetization is connected with more positive value of MAE.

MAE for SVG systems is in the range (-0.29 meV and -0.07 meV), SVNG (-10.10 meV and 1.10 meV), DVG (-1.09 meV and 6.88 meV) and DVNG (-2.10 meV and -0.40 meV). Two results with MAE greater than 1 meV were obtained. Both cases are connected with anisotropy of orbital magnetic moments – for easy axis the increment is 0.013 μ_B (FeSVNG) and 0.126 μ_B (IrDVG). MAE of IrDVG is 6.88 meV, thus it (according to Eq. 26) corresponds to thermal energy of ~ 80 K.

$$E_T = k_B T \tag{26}$$

where T stands for thermodynamic temperature and k_B for Boltzmann constant. This value is comparable with "giant magnetic anisotropy" (~ 9 meV) reported in Ref. [75]. Value

of MAE of IrDVG system obtained by Ref. [70] is much more pronounced (20.79 meV), the difference seems to be related to the applied *k*-point mesh (3 x 3 x 1). Other presented results and DOSs from Ref. [70] are in very good agreement.

MAE of IrSVNG is also worth mentioning. In this case, however, the perpendicular orientation of magnetization is disfavoured by - 10.29 meV. It is once again connected with significant anisotropy of orbital magnetic moments. For out-of-plane orientation of magnetization, the orbital moment is suppressed – the decrement is ~ 0.170 μ_B.

DOSs of IrDVG and IrSVNG are for better understanding of observed MAE shown in Fig. 9, arrows show the states that contribute to the value of MAE. In IrDVG for perpendicular orientation of magnetization, the π_d^* orbital has 2 sharp peaks – one bellow and one above E_F. The peak bellow E_F is more pronounced when the orientation of magnetization is perpendicular to the graphene layer. However, the centres of peaks are similar for both orientations of the magnetic moments, the perpendicular MAE should be also related to the upshift of the deeper-laying states for parallel orientation of magnetization – since peaks for both magnetic orientations slightly vary, it is impossible to assign their individual contribution to MAE.

In IrSVNG the peaks around E_F (π_d^*, δ_d^*) have similar shape in both cases of orientation of magnetization but the peaks corresponding to parallel orientation of magnetization are slightly shifted to the lower energy values. Nevertheless, this shift is again not very significant and the role of deeper laying states must be considered. From the DOS plots it is also apparent that in both IrDVG and IrSVNG the states located on neighbours strictly reflect the states located on Ir adatom in the vicinity of E_F.

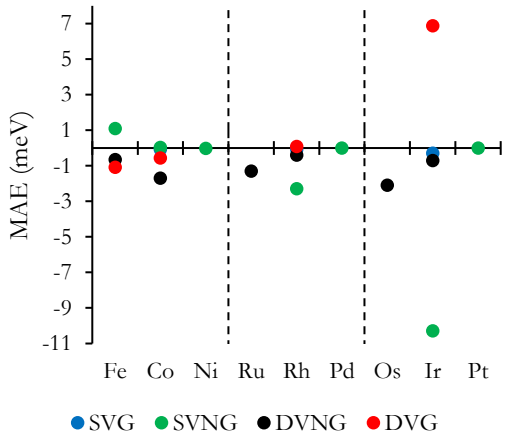

Fig. 8: Values of magnetic anisotropy energy after SOC calculations.

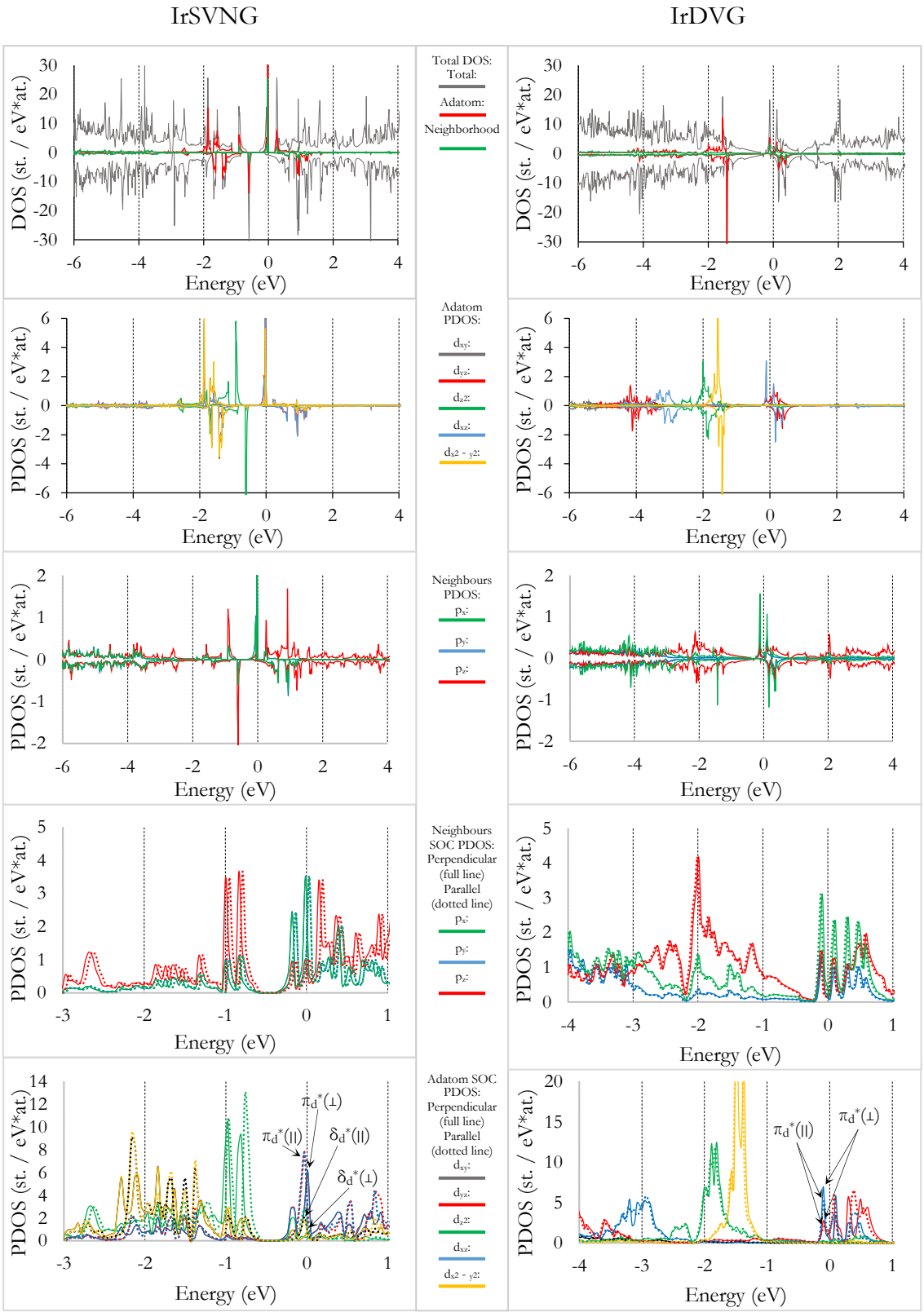

Fig. 9: Total DOS, adatom PDOS, sum of local PDOSs of neighbours, sum of local PDOSs of neighbours from SOC run, adatom PDOS from SOC run. Arrows in the last row point to the areas that contribute to the value of MAE. On the left-hand side is IrSVNG, on the other side is IrDVG.

4 Summary

In this work, a detailed DFT study of structural, electronic and magnetic properties of TM adatoms adsorbed on defective graphene is presented. Geometry relaxations showed that adatom is pulled towards the defect. In SVG and SVNG the adatom after relaxation stayed still significantly above, in DVG closer and in DVNG closest to the graphene plane. The resulting binding is in most cases (except SVNG systems) stronger than 5 eV. Present results revealed that vacancy defects in the graphene can anchor single TM adatoms. Bader charge analysis predicts that all examined adatoms donate electrons to the graphene lattice and therefore they act as *n*-dopants. Trends were analysed in geometry and magnetic properties.

Relativistic calculations including SOC were performed for systems with non-zero values of magnetic moment after SR calculations. Examined systems showed correlation between anisotropy of spin and orbital magnetic moments and MAE. Large MAEs of 6.88 meV and -10.29 meV were found for Ir on DVG and SVNG respectively, accompanied with substantial orbital moment anisotropy (increment 0.126 μ_B and decrement 0.170 μ_B respectively for perpendicular orientation of magnetization). Analysis of PDOSs indicated that the contribution to MAE come from the slight systematic shift of all peaks around E_F to lower energies for parallel orientation of magnetization (IrSVNG) or from change of significance of the peaks around E_F for perpendicular orientation of magnetization (IrDVG). The value of MAE is presumably also related to the deeper-laying states.

Although, the perpendicular MAE of ~ 7 meV is only slightly lower than "giant" magnetic anisotropy of 9 meV experimentally obtained for Co adatoms on Pt(111) reported in Ref. [75], it is still low to be considered as basis for BPM in new generation of HDDs. In this sense the results presented here are preliminary to some extent. The investigations should be continued with the aim of identifying systems with sufficiently high MAEs – transition metal dimers at vacancy defects in graphene may be possible candidates for such high-MAE systems.

References in this field of interest are very scattered and according to my best knowledge, there is lack of some systematic study. Obtained results were in many cases in good agreement with literature, on the other hand, for some systems no reference was found – some results obtained and presented in this thesis are to the best of my knowledge published for the very first time.

5 Závěr

V této bakalářské práci je prezentována detailní DFT studie strukturních, elektronických a magnetických vlastností atomů přechodných kovů adsorbovaných na defektivní grafen. Relaxace geometrie ukázaly, že adatom je vtahován do defektu. V SVG a SVNG adatom po relaxaci zůstal stále významně nad rovinou grafenu, v DVG se dostal blíže a v DVNG nejblíže k rovině grafenu. Výsledná vazba je ve většině případů (kromě SVNG systémů) silnější než 5 eV. Výsledky ukázaly, že defekty mohou ukotvit samostatné atomy přechodných kovů. Analýza Baderových nábojů předpověděla, že všechny zkoumané adatomy přispívají svými elektrony do grafenové mřížky, jedná se tedy o *n*-dopanty. Trendy v geometrických a magnetických vlastnostech byly analyzovány.

Relativistické kalkulace zahrnující SOC byly provedeny pro všechny systémy, které měly nenulové hodnoty magnetických momentů po SR kalkulacích. Ve zkoumaných systémech byla pozorována korelace mezi anizotropií spinových a orbitálních magnetických momentů a MAE. Velké hodnoty MAE 6.88 meV a -10.29 meV byly pozorovány u systémů Ir na DVG a SVNG resp., doprovázeny významnou anizotropií orbitálních magnetických momentů (přírůstek 0.126 μ_B a úbytek 0.170 μ_B resp. pro kolmou orientaci magnetizace). Analýza PDOS ukázala, že příspěvky k MAE pocházejí z mírného systematického posunu všech píků v blízkosti E_F k nižším energiím pro paralelní orientaci magnetizace (IrSVNG) nebo ze změny velikosti píků v okolí E_F pro kolmou orientaci magnetizace (IrDVG). Hodnota MAE pravděpodobně souvisí také s hlouběji umístěnými stavy.

I když hodnota kolmé MAE ~ 7 meV je pouze o trochu menší než "obrovská" magnetická anizotropie 9 meV experimentálně naměřená pro atomy Co na Pt(111) v Ref. [75], je to stále příliš málo, aby tento systém mohl být považován za základ BPM v nové generaci HDD. Kvůli tomu je nutné výsledky dále rozšířit – další výzkumy by měly pokračovat s cílem popsat systémy s dostatečně velkými hodnotami MAE – dimery přechodných kovů by mohly být vhodnými kandidáty.

Informační zdroje jsou v této oblasti zájmu velice rozptýlené a dle mých nejlepších znalostí neexistuje žádná systematická studie. Obdržené výsledky byly v mnoha případech v dobrém souladu s literaturou, na druhou stranu pro některé výsledky nebyla žádná reference nalezena – některé výsledky obdržené a uvedené v této práci jsou pravděpodobně publikovány úplně poprvé.

6 Bibliography

(1) Feynman, R. There's Plenty of Room at the Bottom, 1959.

(2) Gantz, J.; Reinsel, D. *IDC* **2012**, 1–16.

(3) Fontana, R. E.; Decad, G. M. *AIP Adv.* **2018**, *8* (5), 056506.

(4) Wood, R. *IEEE Trans. Magn.* **2000**, *36* (1), 36–42.

(5) Shiroishi, Y.; Fukuda, K.; Tagawa, I.; Iwasaki, H.; Takenoiri, S.; Tanaka, H.; Mutoh, H.; Yoshikawa, N. *IEEE Trans. Magn.* **2009**, *45* (10), 3816–3822.

(6) Natterer, F. D.; Yang, K.; Paul, W.; Willke, P.; Choi, T.; Greber, T.; Heinrich, A. J.; Lutz, C. P. *Nature* **2017**, *543* (7644), 226–228.

(7) Baltic, R.; Pivetta, M.; Donati, F.; Wäckerlin, C.; Singha, A.; Dreiser, J.; Rusponi, S.; Brune, H. *Nano Lett.* **2016**, *16* (12), 7610–7615.

(8) Błoński, P.; Hafner, J. *Phys. Rev. B* **2009**, *79* (22), 224418.

(9) Błoński, P.; Hafner, J. *J. Phys. Condens. Matter* **2014**, *26* (14), 146002.

(10) Błoński, P.; Hafner, J. *J. Phys. Condens. Matter* **2014**, *26* (25), 256001.

(11) Gan, Y.; Sun, L.; Banhart, F. *Small* **2008**, *4* (5), 587–591.

(12) Bakandritsos, A.; Kadam, R. G.; Kumar, P.; Zoppellaro, G.; Medved', M.; Tuček, J.; Montini, T.; Tomanec, O.; Andrýsková, P.; Drahoš, B.; Varma, R. S.; Otyepka, M.; Gawande, M. B.; Fornasiero, P.; Zbořil, R. *Adv. Mater.* **2019**, *1900323*, 1900323.

(13) Yang, X. F.; Wang, A.; Qiao, B.; Li, J.; Liu, J.; Zhang, T. *Acc. Chem. Res.* **2013**, *46* (8), 1740–1748.

(14) Wikipedia. Hard disk drive. https://en.wikipedia.org/wiki/Hard_disk_drive (accessed January 6, 2019).

(15) Wikipedia. Solid-state drive. https://en.wikipedia.org/wiki/Solid-state_drive (accessed January 6, 2019).

(16) Plumer, M. L.; van Ek, J.; Cain, W. C. *La Phys. au Canada* **2011**, *67* (1), 25–29.

(17) Kubota, Y.; Folks, L.; Marinero, E. E. *J. Appl. Phys.* **1998**, *84* (11), 6202–6207.

(18) Donati, F.; Rusponi, S.; Stepanow, S.; Wackerlin, C.; Singha, A.; Persichetti, L.; Baltic, R.; Diller, K.; Patthey, F.; Fernandes, E.; Dreiser, J.; ljivan anin, .; Kummer, K.; Nistor, C.; Gambardella, P.; Brune, H. *Science (80-.).* **2016**, *352* (6283), 318–321.

(19) Sessoli, R. *Nature* **2017**, *543* (7644), 189–190.

(20) Natterer, F. D.; Donati, F.; Patthey, F.; Brune, H. *Phys. Rev. Lett.* **2018**, *121* (2), 027201.

(21) Novoselov, K. S.; Geim, A. K.; Morozov, S. V.; Jiang, D.; Zhang, Y.; Dubonos, S. V.; Grigorieva, I. V.; Firsov, A. A. *Science (80-.).* **2004**, *306* (5696), 666–669.

(22) Ashton, M.; Paul, J.; Sinnott, S. B.; Hennig, R. G. *Phys. Rev. Lett.* **2017**, *118* (10), 106101.

(23) Tuček, J.; Błoński, P.; Ugolotti, J.; Swain, A. K.; Enoki, T.; Zbořil, R. *Chem. Soc. Rev.* **2018**, *47* (11), 3899–3990.

(24) Lee, C.; Wei, X.; Kysar, J. W.; Hone, J. *Science (80-.).* **2008**, *321* (5887), 385–388.

(25) Balandin, A. A.; Ghosh, S.; Bao, W.; Calizo, I.; Teweldebrhan, D.; Miao, F.; Lau, C. N. *Nano Lett.* **2008**, *8* (3), 902–907.

(26) Cai, W.; Moore, A. L.; Zhu, Y.; Li, X.; Chen, S.; Shi, L.; Ruoff, R. S. *Nano Lett.* **2010**, *10* (5), 1645–1651.

(27) Bolotin, K. I.; Sikes, K. J.; Jiang, Z.; Klima, M.; Fudenberg, G.; Hone, J.; Kim, P.; Stormer, H. L. *Solid State Commun.* **2008**, *146* (9–10), 351–355.

(28) Li, Z.; Chen, L.; Meng, S.; Guo, L.; Huang, J.; Liu, Y.; Wang, W.; Chen, X. *Phys. Rev. B* **2015**, *91* (9), 094429.

(29) Nair, R. R.; Ren, W.; Jalil, R.; Riaz, I.; Kravets, V. G.; Britnell, L.; Blake, P.; Schedin, F.; Mayorov, A. S.; Yuan, S.; Katsnelson, M. I.; Cheng, H.-M.; Strupinski, W.; Bulusheva, L. G.; Okotrub, A. V.; Grigorieva, I. V.; Grigorenko, A. N.; Novoselov, K. S.; Geim, A. K. *Small* **2010**, *6* (24), 2877–2884.

(30) A Abdala, A. *J. Biofertilizers Biopestic.* **2014**, *05* (01).

(31) Srivastava, A.; Rastogi, S.; Verma, A.; Singh, P. *Int. J. Adv. Res. Sci. Eng.* **2015**, *4* (1), 49–53.

(32) Dai, X. Q.; Zhao, J. H.; Xie, M. H.; Tang, Y. N.; Li, Y. H.; Zhao, B. *Eur. Phys. J. B* **2011**, *80* (3), 343–349.

(33) Fujimoto, Y.; Saito, S. *Phys. Rev. B* **2011**, *84* (24), 245446.

(34) Hou, Z.; Wang, X.; Ikeda, T.; Terakura, K.; Oshima, M.; Kakimoto, M. *Phys. Rev. B* **2013**, *87* (16), 165401.

(35) Hou, Z.; Wang, X.; Ikeda, T.; Terakura, K.; Oshima, M.; Kakimoto, M. A.; Miyata, S. *Phys. Rev. B - Condens. Matter Mater. Phys.* **2012**, *85* (16), 1–9.

(36) Lin, Y.-C.; Teng, P.-Y.; Yeh, C.-H.; Koshino, M.; Chiu, P.-W.; Suenaga, K. *Nano Lett.* **2015**, *15* (11), 7408–7413.

(37) Groß, A. *Theoretical Surface Science*; Springer Berlin Heidelberg: Berlin, Heidelberg,

2009.

(38) Hobbs, D.; Kresse, G.; Hafner, J. *Phys. Rev. B - Condens. Matter Mater. Phys.* **2000**, *62* (17), 11556–11570.

(39) Kresse, G.; Hafner, J. *Phys. Rev. B* **1993**, *47* (1), 558–561.

(40) Kresse, G.; Furthmüller, J. *Comput. Mater. Sci.* **1996**, *6* (1), 15–50.

(41) Kresse, G.; Furthmüller, J. *Phys. Rev. B* **1996**, *54* (16), 11169–11186.

(42) Kresse, G.; Joubert, D. *Phys. Rev. B* **1999**, *59* (3), 1758–1775.

(43) Perdew, J. P.; Burke, K.; Ernzerhof, M. *Phys. Rev. Lett.* **1996**, *77* (18), 3865–3868.

(44) Bader, R. F. W. *Acc. Chem. Res.* **1985**, *18* (1), 9–15.

(45) Bader, R. F. W.; Nguyen-Dang, T. T. *Adv. Quantum Chem.* **1981**, *14*, 63–124.

(46) Henkelman, G.; Arnaldsson, A.; Jónsson, H. *Comput. Mater. Sci.* **2006**, *36* (3), 354–360.

(47) Manadé, M.; Viñes, F.; Illas, F. *Carbon N. Y.* **2015**, *95*, 525–534.

(48) Rodrigo, L.; Pou, P.; Pérez, R. *Carbon N. Y.* **2016**, *103*, 200–208.

(49) Choi, W. I.; Jhi, S. H.; Kim, K.; Kim, Y. H. *Phys. Rev. B - Condens. Matter Mater. Phys.* **2010**, *81* (8), 1–5.

(50) Gao, Z.; Yang, W.; Ding, X.-L.; Lv, G.; Yan, W. *Phys. Chem. Chem. Phys.* **2018**, *20* (10), 7333–7341.

(51) Krasheninnikov, A. V.; Lehtinen, P. O.; Foster, A. S.; Pyykkö, P.; Nieminen, R. M. *Phys. Rev. Lett.* **2009**, *102* (12), 126807.

(52) Raji, A. T.; Lombardi, E. B. *Phys. B Condens. Matter* **2015**, *464*, 28–37.

(53) Santos, E. J. G.; Ayuela, A.; Sanchez-Portal, D. **2009**.

(54) Sun, M.; Ren, Q.; Zhao, Y.; Chou, J.-P.; Yu, J.; Tang, W. *Carbon N. Y.* **2017**, *120*, 265–273.

(55) Guo, X.; Liu, S.; Huang, S. *Int. J. Hydrogen Energy* **2018**, *43* (10), 4880–4892.

(56) Ambrusi, R. E.; Luna, C. R.; Juan, A.; Pronsato, M. E. *RSC Adv.* **2016**, *6* (87), 83926–83941.

(57) Zhou, Q.; Wang, C.; Fu, Z.; Yuan, L.; Yang, X.; Tang, Y.; Zhang, H. *Int. J. Hydrogen Energy* **2015**, *40* (6), 2473–2483.

(58) Ma, L.; Zhang, J.-M.; Xu, K.-W.; Ji, V. *Phys. E Low-dimensional Syst. Nanostructures* **2015**, *66*, 40–47.

(59) Sun, M.; Tang, W.; Ren, Q.; Zhao, Y.; Wang, S.; Yu, J.; Du, Y.; Hao, Y. *Phys. E Low-dimensional Syst. Nanostructures* **2016**, *80*, 142–148.

(60) Han, Y.; Ge, G.-X.; Wan, J.-G.; Zhao, J.-J.; Song, F.-Q.; Wang, G.-H. *Phys. Rev. B* **2013**, *87* (15), 155408.

(61) Fampiou, I.; Ramasubramaniam, A. *J. Phys. Chem. C* **2012**, *116* (11), 6543–6555.

(62) Kattel, S.; Atanassov, P.; Kiefer, B. *J. Phys. Chem. C* **2012**, *116* (14), 8161–8166.

(63) Zhang, X.; Lu, Z.; Yang, Z. *J. Mol. Catal. A Chem.* **2016**, *417*, 28–35.

(64) Yang, M.; Wang, L.; Li, M.; Hou, T.; Li, Y. *AIP Adv.* **2015**, *5* (6), 067136.

(65) Zhou, X.; Chu, W.; Sun, W.; Zhou, Y.; Xue, Y. *Comput. Theor. Chem.* **2017**, *1120*, 8–16.

(66) Zhao, C.; Wu, H. *Appl. Surf. Sci.* **2018**, *435*, 1199–1212.

(67) Rangel, E.; Sansores, E. *Int. J. Hydrogen Energy* **2014**, *39* (12), 6558–6566.

(68) Rafique, M.; Shuai, Y.; Xu, M.; Zhang, G.; Guo, Y. *Phys. E Low-dimensional Syst. Nanostructures* **2017**, *93* (February), 26–38.

(69) Rafique, M.; Shuai, Y.; Tan, H.; Hassan, M. *Chinese Phys. B* **2017**, *26* (5), 056301.

(70) Ge, G.-X.; Li, Y.-B.; Wang, G.-H.; Wan, J.-G. *Phys. Chem. Chem. Phys.* **2016**, *18* (16), 11550–11555.

(71) Václavková, D. Magnetic anisotropy of transition metal dimers supported by defective graphene, Palacký University Olomouc, 2018.

(72) Back, S.; Lim, J.; Kim, N.-Y.; Kim, Y.-H.; Jung, Y. *Chem. Sci.* **2017**, *8* (2), 1090–1096.

(73) Tang, Y.; Zhou, J.; Shen, Z.; Chen, W.; Li, C.; Dai, X. *RSC Adv.* **2016**, *6* (96), 93985–93996.

(74) Fair, K. M.; Cui, X. Y.; Li, L.; Shieh, C. C.; Zheng, R. K.; Liu, Z. W.; Delley, B.; Ford, M. J.; Ringer, S. P.; Stampfl, C. *Phys. Rev. B - Condens. Matter Mater. Phys.* **2013**, *87* (1), 1–7.

(75) Gambardella, P.; Rusponi, S.; Veronese, M.; Dhesi, S. S.; Grazioli, C.; Dallmeyer, A.; Cabria, I.; Zeller, R.; Dederichs, P. H.; Kern, K.; Carbone, C.; Brune, H. *Science (80-.).* **2003**, *300* (5622), 1130–1133.

7 Appendices

7.1 Appendix 1: Tables with obtained values

Tab. A1: Average bond lengths (adatom – neighbour) in vacancy graphene systems.

	Average bond length (adatom - neighbour) (Å)			
	SVG	SVNG	DVG	DVNG
Fe	1.766	1.867	1.952	1.900
Co	1.766	1.828	1.935	1.881
Ni	1.794	1.837	1.885	1.885
Ru	1.882	1.917	2.023	1.963
Rh	1.896	2.037	2.024	1.947
Pd	1.943	2.175	1.999	1.954
Os	1.893	1.913	2.022	1.947
Ir	1.904	2.011	2.009	1.948
Pt	1.934	2.153	1.985	1.956

Tab. A2: Vertical distance (adatom – neighbour) in vacancy graphene systems.

	Vertical distances (adatom - neighbour) (Å)			
	SVG	SVNG	DVG	DVNG
Fe	0.889	0.951	0.434	0.006
Co	0.890	0.866	0.487	0.002
Ni	0.939	0.870	0.161	0.002
Ru	1.043	1.067	0.758	0.238
Rh	1.064	1.329	0.686	0.044
Pd	1.150	1.433	0.454	0.017
Os	1.035	1.019	0.738	0.164
Ir	1.050	1.278	0.607	0.022
Pt	1.104	1.403	0.370	0.001

Tab. A3: Graphene buckling amplitude (Å) after adatom bonding in vacancy graphene systems.

	Graphene buckling amplitude (Å)			
	SVG	SVNG	DVG	DVNG
Fe	0.508	0.542	0.187	0.017
Co	0.479	0.514	0.130	0.000
Ni	0.336	0.610	0.158	0.000
Ru	0.662	0.471	0.200	0.198
Rh	0.578	0.283	0.187	0.115
Pd	0.469	0.323	0.405	0.057
Os	0.725	0.550	0.245	0.209
Ir	0.655	0.368	0.386	0.046
Pt	0.555	0.355	0.489	0.002

Tab. A4: Local magnetic moment of adatom in defective graphene systems.

	Adatom local magnetic moment (μ_B)			
	SVG	SVNG	DVG	DVNG
Fe	0.000	3.002	2.834	1.921
Co	0.317	1.880	0.998	0.701
Ni	0.000	1.152	0.000	0.000
Ru	0.000	0.000	0.000	1.274
Rh	0.204	0.978	0.475	0.155
Pd	0.000	0.543	0.000	0.000
Os	0.000	0.000	0.000	0.154
Ir	0.265	0.740	0.353	0.279
Pt	0.000	0.533	0.000	0.000

Tab. A5: Sum of local magnetic moments of atoms of defective graphene.

	Defective graphene magnetic moment (μ_B)			
	SVG	SVNG	DVG	DVNG
Fe	0.000	-0.080	0.225	-0.075
Co	0.286	0.104	-0.017	0.029
Ni	0.000	0.260	0.000	0.000
Ru	0.000	0.000	0.000	0.147
Rh	0.368	0.580	0.251	0.051
Pd	0.000	0.315	0.000	0.000
Os	0.000	0.000	0.000	-0.014
Ir	0.299	0.551	0.269	0.105
Pt	0.000	0.290	0.000	0.000

Tab. A6: Second biggest local magnetic moment of any atom in defective graphene systems.

	Second biggest magnetic moment (μ_B)			
	SVG	SVNG	DVG	DVNG
Fe	0.000	0.050	0.022	0.016
Co	0.042	0.061	0.008	0.009
Ni	0.000	0.098	0.000	0.000
Ru	0.000	0.000	0.000	0.018
Rh	0.052	0.121	0.036	0.006
Pd	0.000	0.134	0.000	0.000
Os	0.000	0.000	0.000	0.004
Ir	0.048	0.105	0.035	0.010
Pt	0.000	0.130	0.000	0.000

Tab. A7: Values of magnetic anisotropy energy after SOC calculations.

	Magnetic anisotropy energy (meV)			
	SVG	SVNG	DVG	DVNG
Fe		1.10	-1.09	-0.66
Co	-0.07	0.04	-0.56	-1.69
Ni		-0.02		
Ru				-1.30
Rh	-0.07	-2.29	0.09	-0.40
Pd		-0.01		
Os				-2.10
Ir	-0.29	-10.29	6.88	-0.71
Pt		0.00		

Tab. A8: Change of spin magnetic moment of adatom (μ_B, positive value stands for increment in perpendicular orientation).

	Spin magnetic moment difference (μ_B)			
	SVG	SVNG	DVG	DVNG
Fe	-0.001	-0.001		0.000
Co	-0.004	-0.008	0.000	-0.001
Ni				0.000
Ru		-0.006		
Rh	0.008	-0.046	-0.001	-0.001
Pd				0.003
Os		-0.042		
Ir	0.105	-0.081	-0.017	-0.035
Pt				0.042

Tab. A9: Change of orbital magnetic moment of adatom (μ_B, positive value stands for increment in perpendicular orientation).

	Orbital magnetic moment difference (μ_B)			
	SVG	SVNG	DVG	DVNG
Fe	0.000	-0.090		0.013
Co	-0.104	-0.207	-0.003	-0.014
Ni				0.003
Ru		-0.092		
Rh	0.062	-0.171	-0.003	-0.083
Pd				-0.027
Os		-0.037		
Ir	0.126	-0.312	-0.020	-0.178
Pt				0.001

7.2 Appendix 2: Graphical summary of each system

In this part each examined system is completely described at one place. At first, top and side views are presented. In top-view figure also bond lengths between adatom and its neighbours are shown. In side-view figure the vertical distances are shown – the different criterions for vertical distance evaluation were described in subchapter 2.2. Next, the Bader charges located on each atom and charge density difference (isosurface = 0.007) are shown in one figure. Green (red) regions show regions with increased (decreased) electron density after the adatom bonding. Three figures from different angles and with isosurface values suitable for each system are then plotted. Other given results should be self-explanatory.

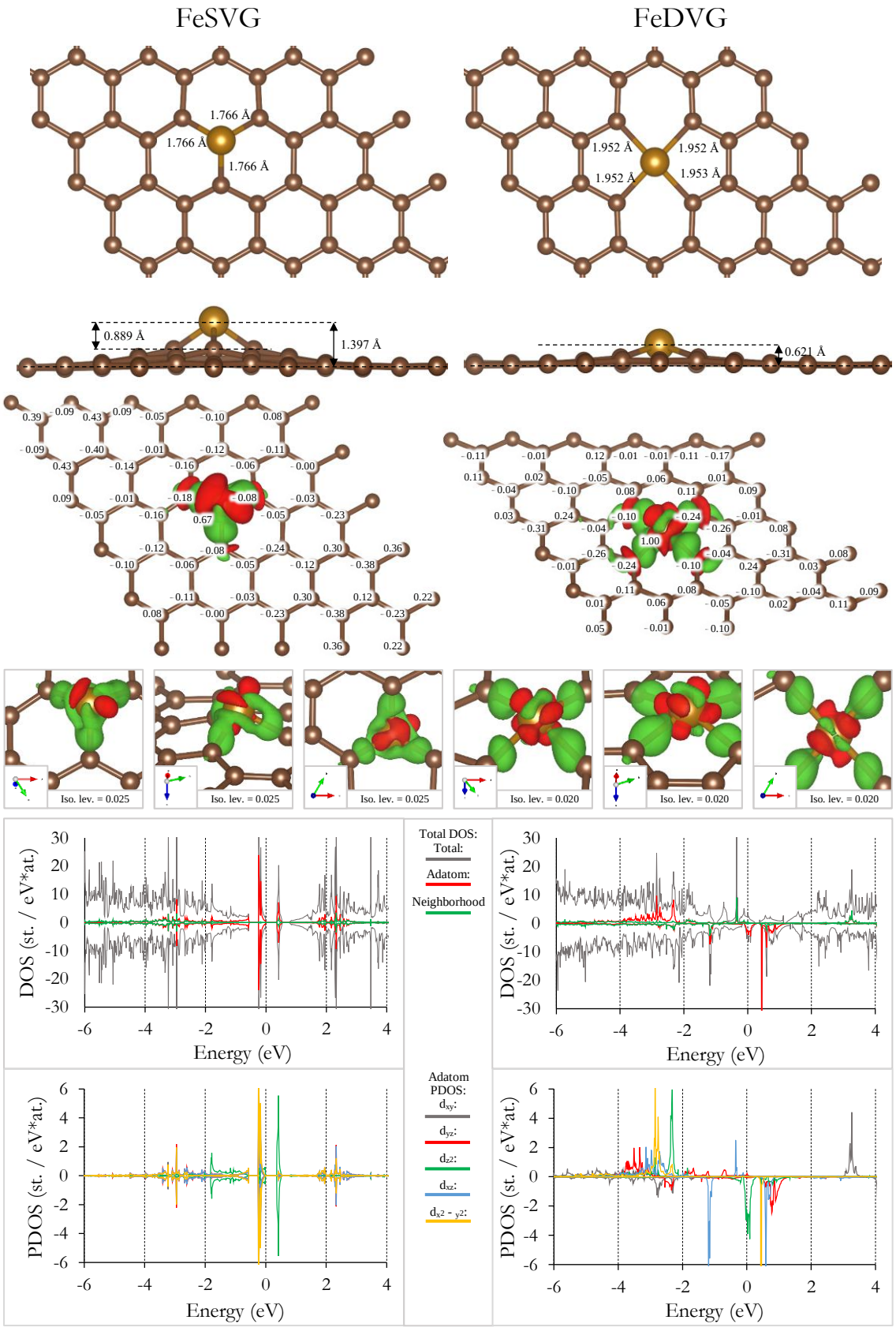

Adsorption energy: -7.150 eV
Total magnetic moment: 0.000 μ_B
Adatom magnetic moment: 0.000 μ_B
Graphene magnetic moment: 0.000 μ_B
Second biggest magnetic moment: 0.000 μ_B

Adsorption energy: -6.095 eV
Total magnetic moment: 3.388 μ_B
Adatom magnetic moment: 2.834 μ_B
Graphene magnetic moment: 0.225 μ_B
Second biggest magnetic moment: 0.022 μ_B

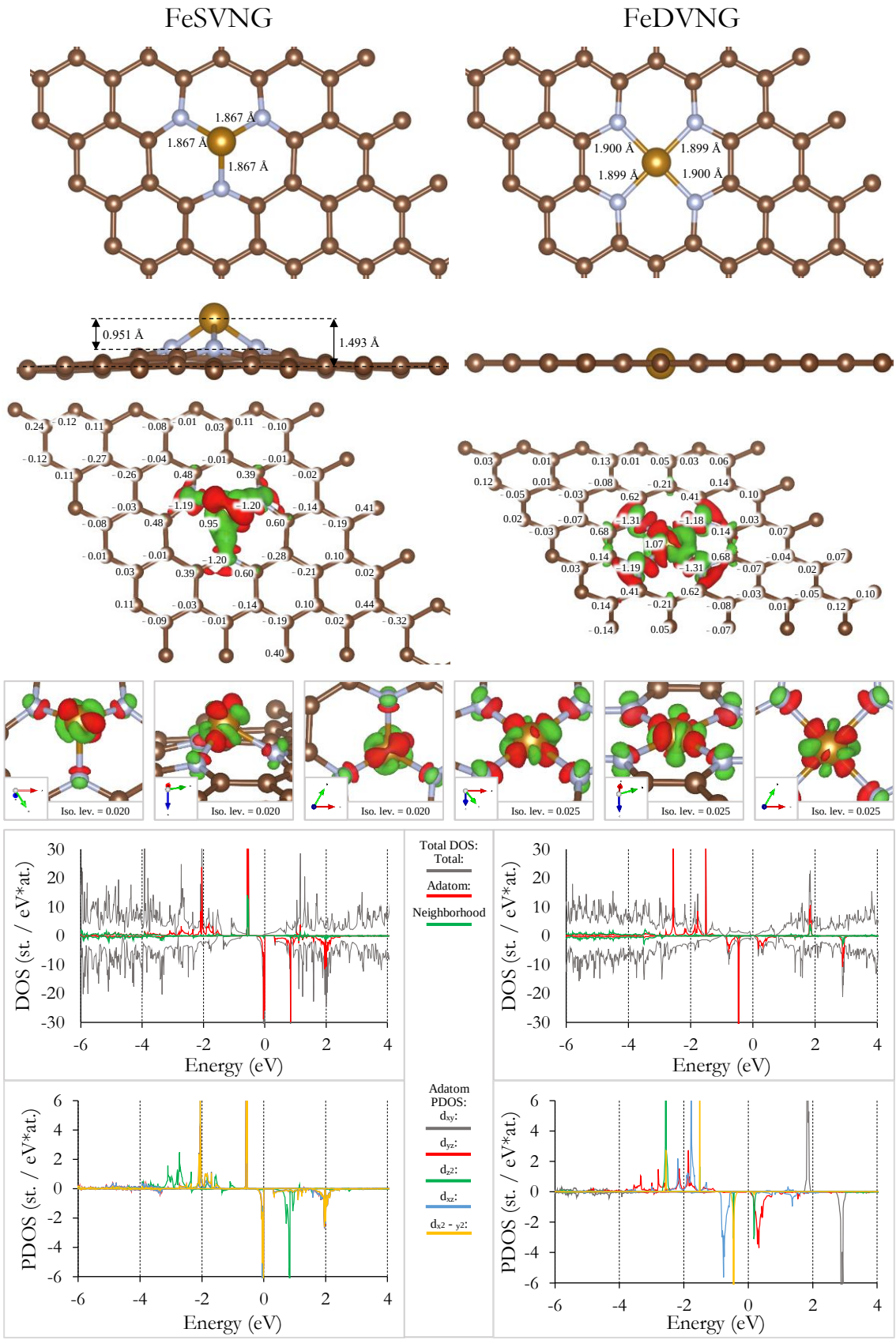

Adsorption energy: -4.479 eV
Total magnetic moment: 3.070 μ_B
Adatom magnetic moment: 3.002 μ_B
Graphene magnetic moment: -0.080 μ_B
Second biggest magnetic moment: 0.050 μ_B

Adsorption energy: -7.228 eV
Total magnetic moment: 2.000 μ_B
Adatom magnetic moment: 1.921 μ_B
Graphene magnetic moment: -0.075 μ_B
Second biggest magnetic moment: -0.016 μ_B

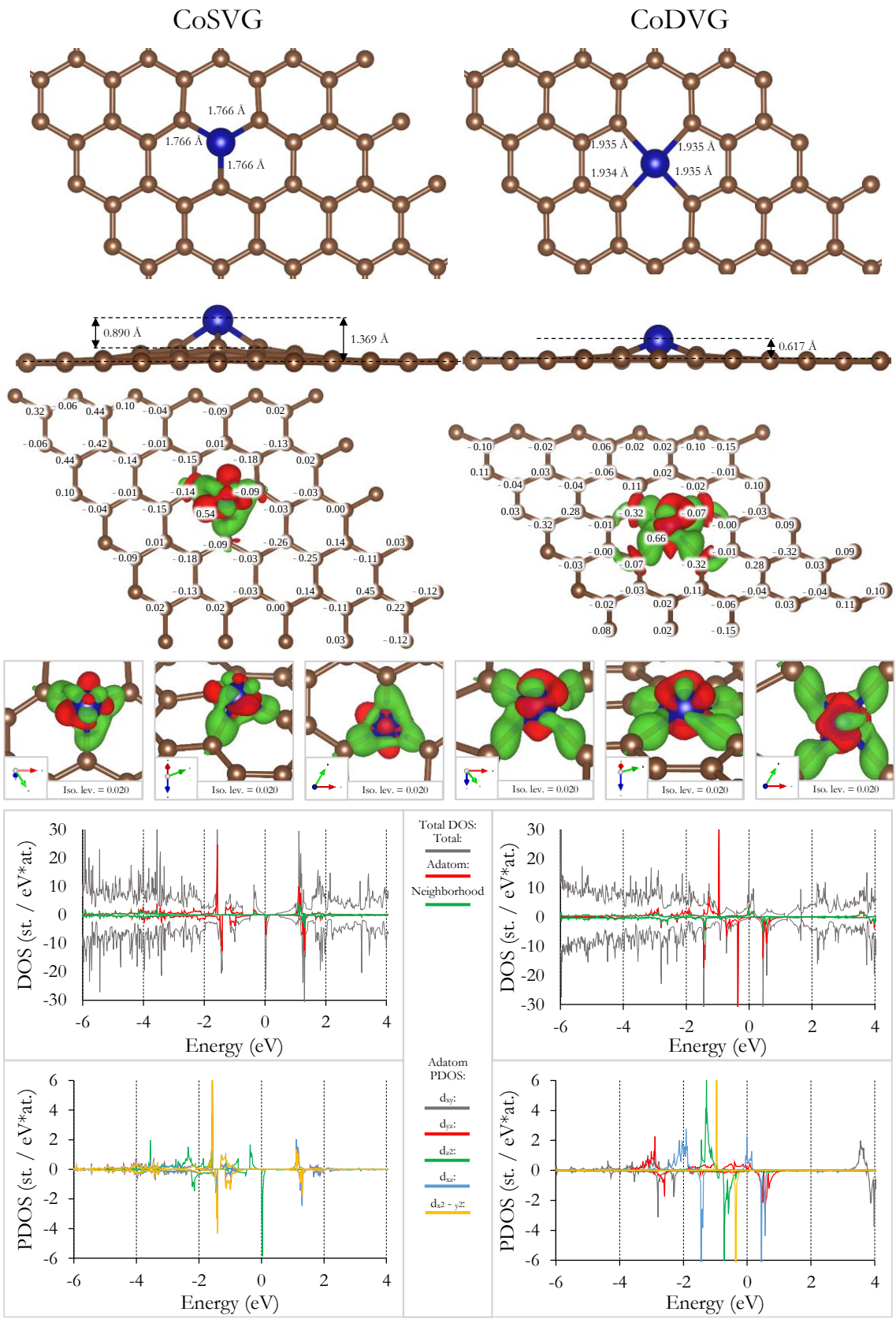

Adsorption energy: -7.635 eV
Total magnetic moment: 0.997 μ_B
Adatom magnetic moment: 0.317 μ_B
Graphene magnetic moment: 0.286 μ_B
Second biggest magnetic moment: 0.042 μ_B

Adsorption energy: -6.406 eV
Total magnetic moment: 1.050 μ_B
Adatom magnetic moment: 0.998 μ_B
Graphene magnetic moment: -0.017 μ_B
Second biggest magnetic moment: 0.008 μ_B

CoSVNG

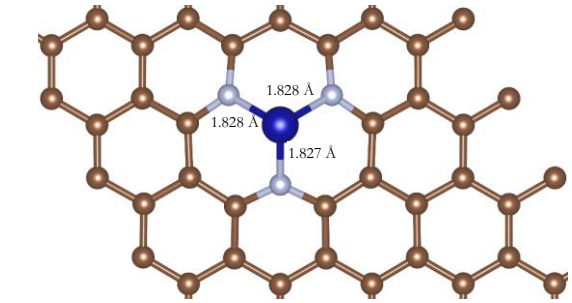

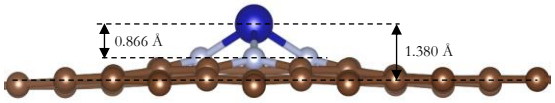

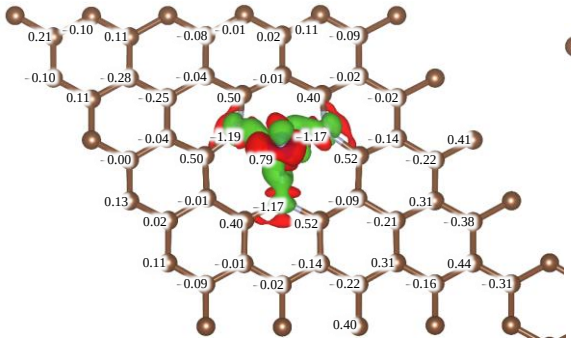

CoDVNG

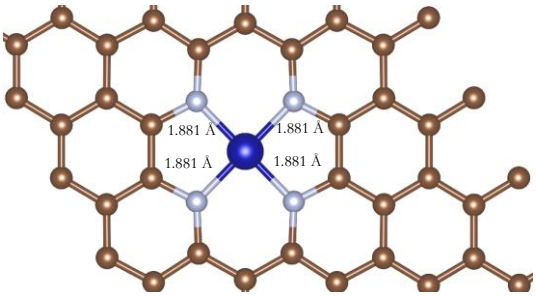

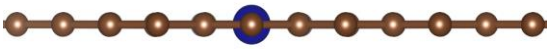

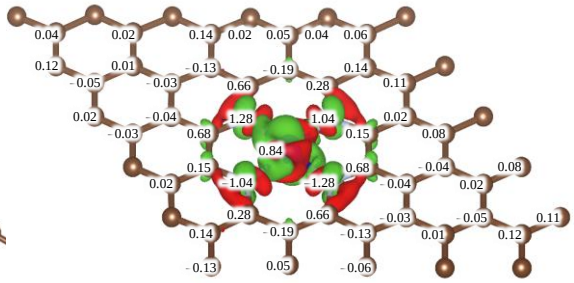

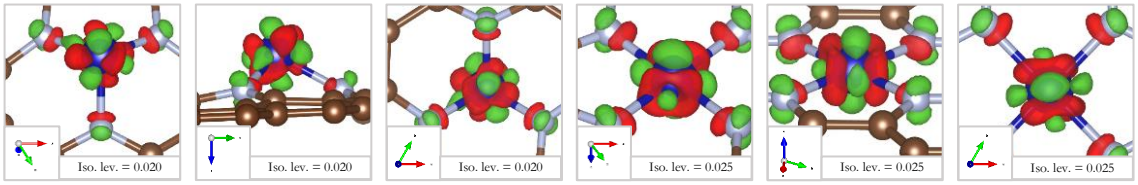

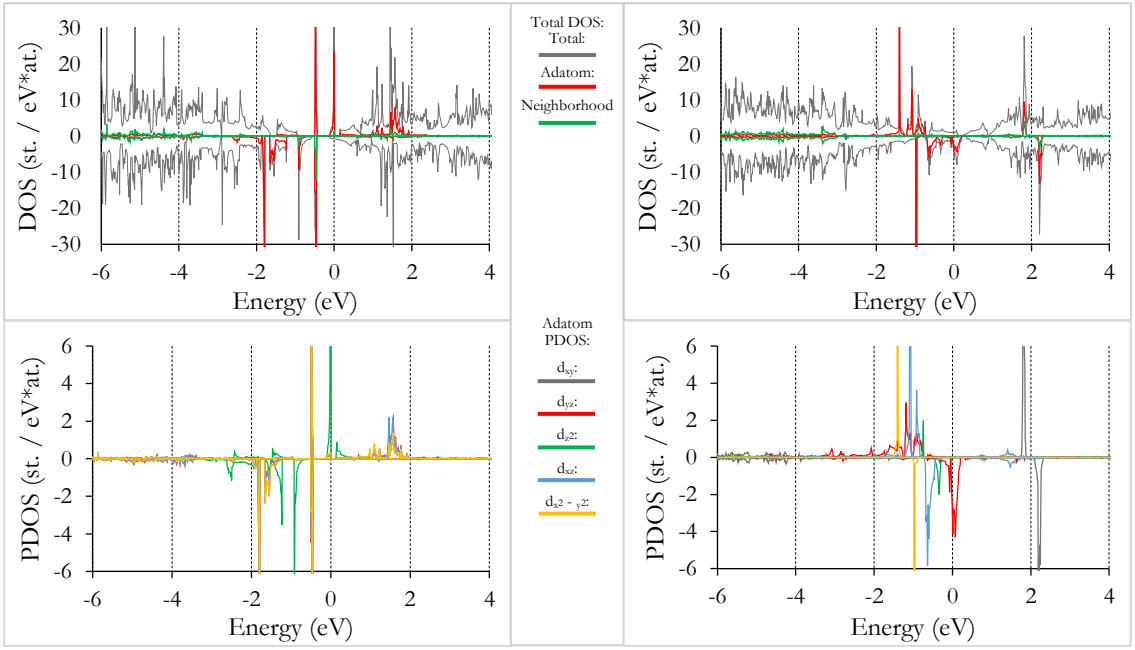

Adsorption energy: -4.875 eV
Total magnetic moment: 2.162 μ_B
Adatom magnetic moment: 1.880 μ_B
Graphene magnetic moment: 0.104 μ_B
Second biggest magnetic moment: 0.061 μ_B

Adsorption energy: -7.674 eV
Total magnetic moment: -0.772 μ_B
Adatom magnetic moment: -0.701 μ_B
Graphene magnetic moment: 0.029 μ_B
Second biggest magnetic moment: -0.009 μ_B

NiSVG

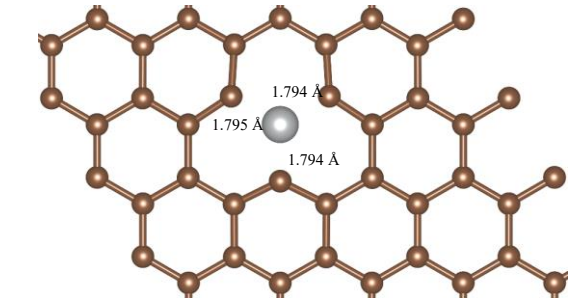

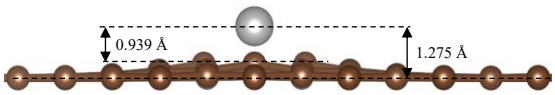

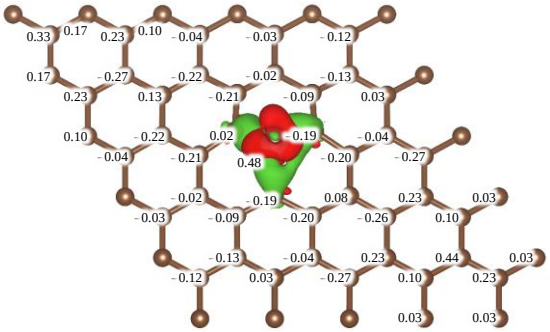

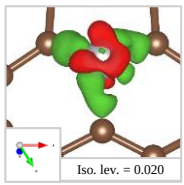

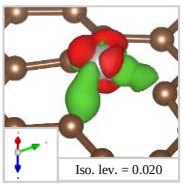

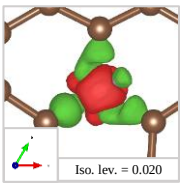

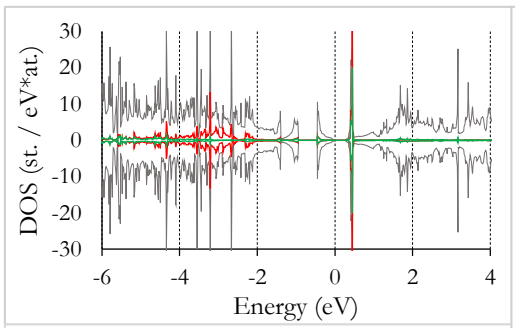

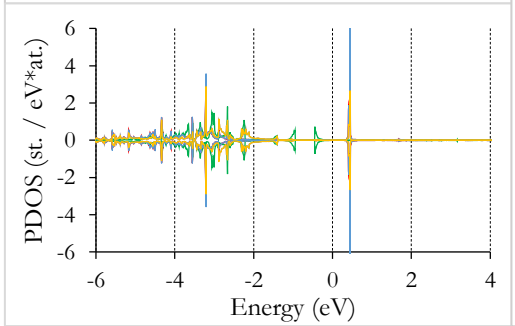

Adsorption energy: -6.734 eV
Total magnetic moment: 0.000 μB
Adatom magnetic moment: -0.000 μB
Graphene magnetic moment: 0.000 μB
Second biggest magnetic moment: 0.000 μB

NiDVG

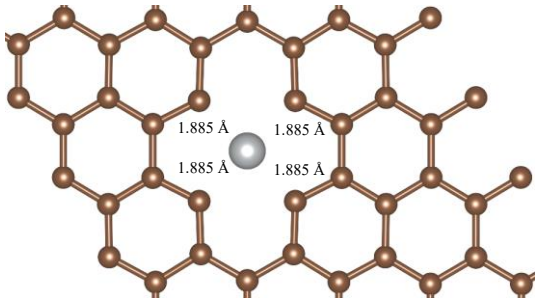

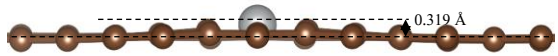

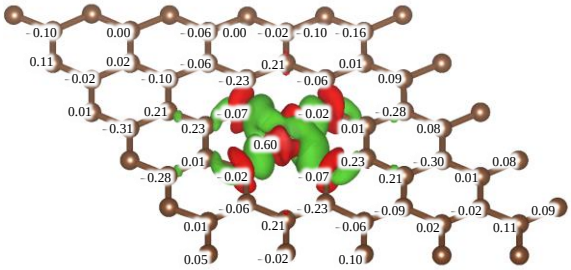

Adsorption energy: -6.461 eV
Total magnetic moment: 0.000 μB
Adatom magnetic moment: -0.000 μB
Graphene magnetic moment: 0.000 μB
Second biggest magnetic moment: 0.000 μB

NiSVNG

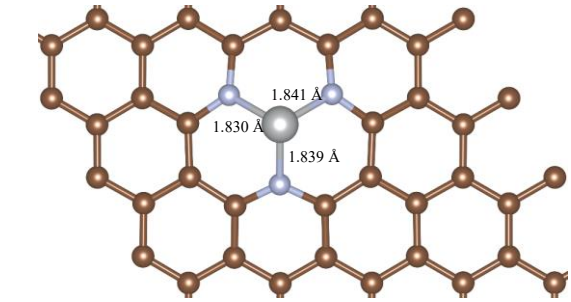

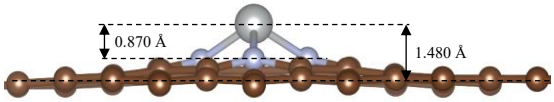

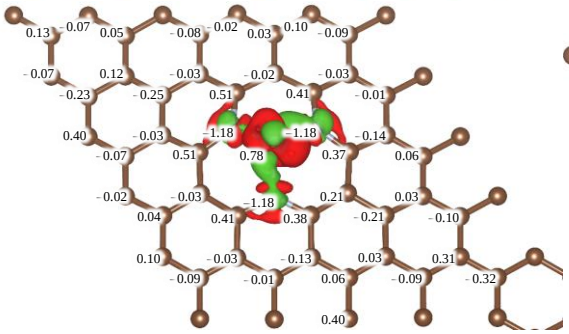

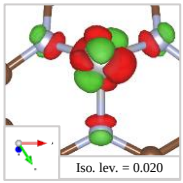

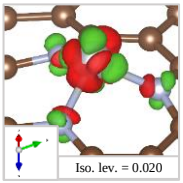

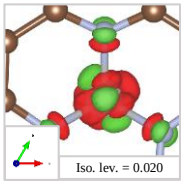

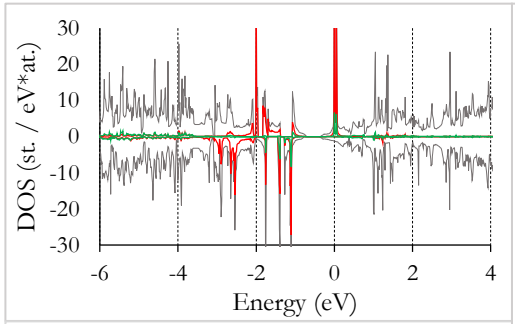

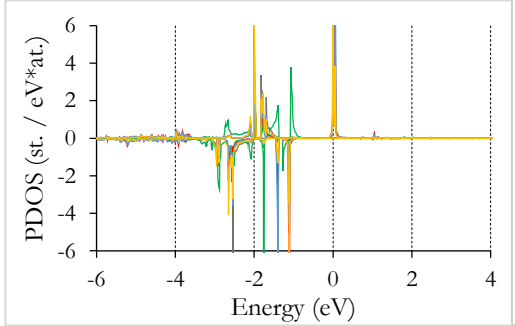

Adsorption energy: -4.419 eV
Total magnetic moment: -1.570 μ_B
Adatom magnetic moment: -1.152 μ_B
Graphene magnetic moment: -0.260 μ_B
Second biggest magnetic moment: -0.098 μ_B

NiDVNG

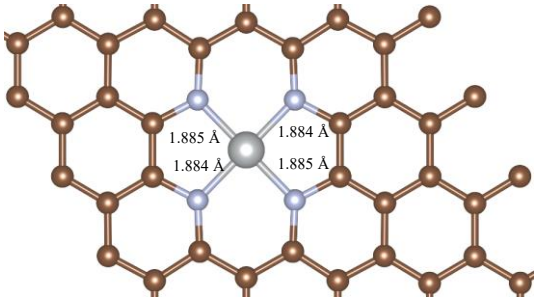

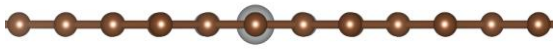

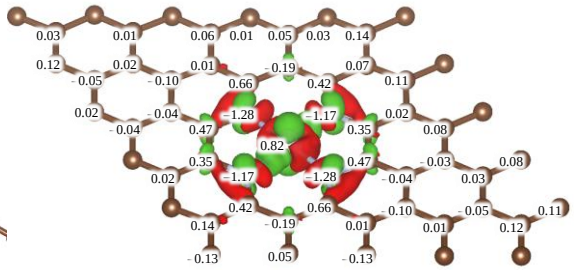

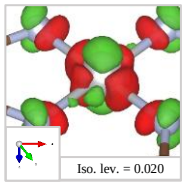

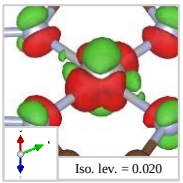

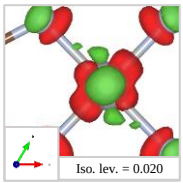

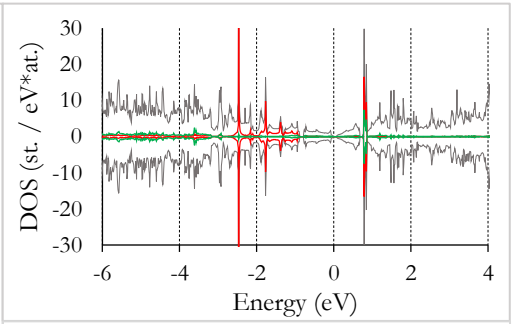

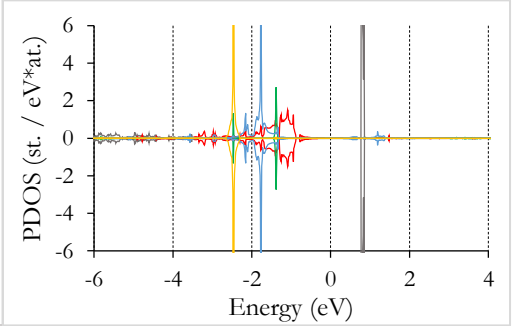

Adsorption energy: -7.644 eV
Total magnetic moment: -0.000 μ_B
Adatom magnetic moment: 0.000 μ_B
Graphene magnetic moment: 0.000 μ_B
Second biggest magnetic moment: 0.000 μ_B

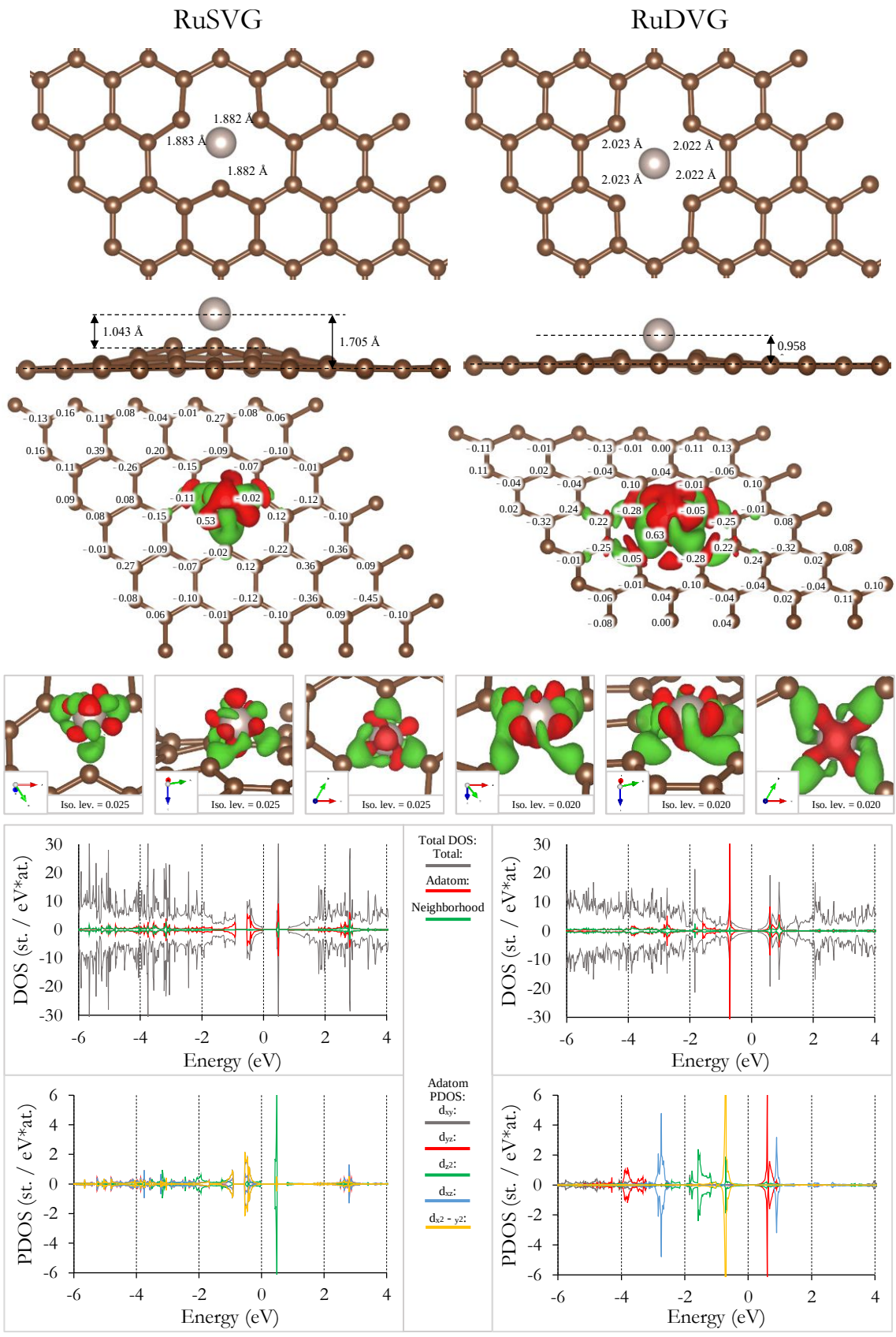

Adsorption energy: -8.792 eV
Total magnetic moment: 0.000 μ_B
Adatom magnetic moment: -0.000 μ_B
Graphene magnetic moment: 0.000 μ_B
Second biggest magnetic moment: 0.000 μ_B

Adsorption energy: -8.030 eV
Total magnetic moment: -0.000 μ_B
Adatom magnetic moment: 0.000 μ_B
Graphene magnetic moment: 0.000 μ_B
Second biggest magnetic moment: 0.000 μ_B

RuSVNG

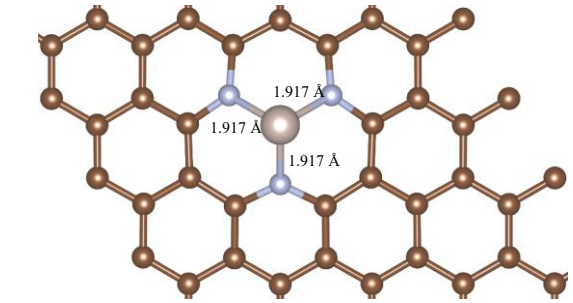

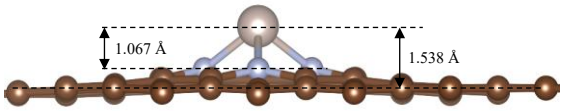

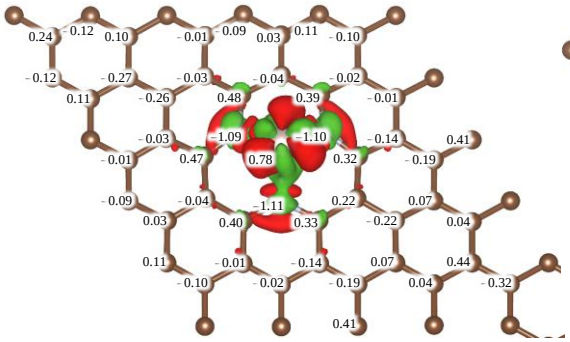

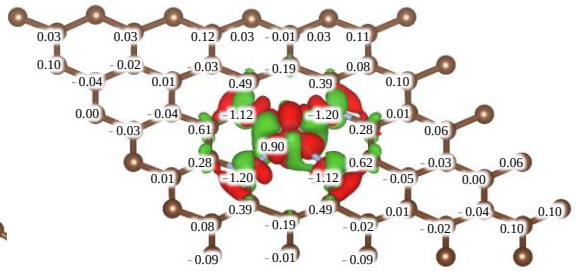

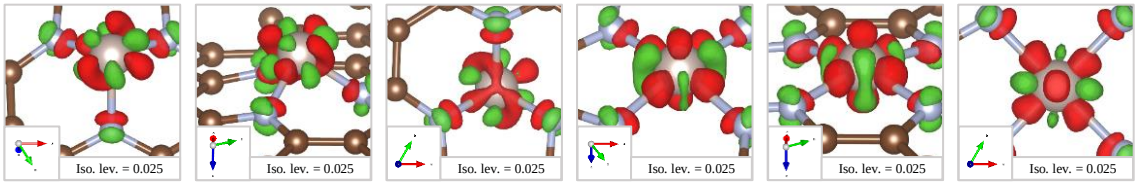

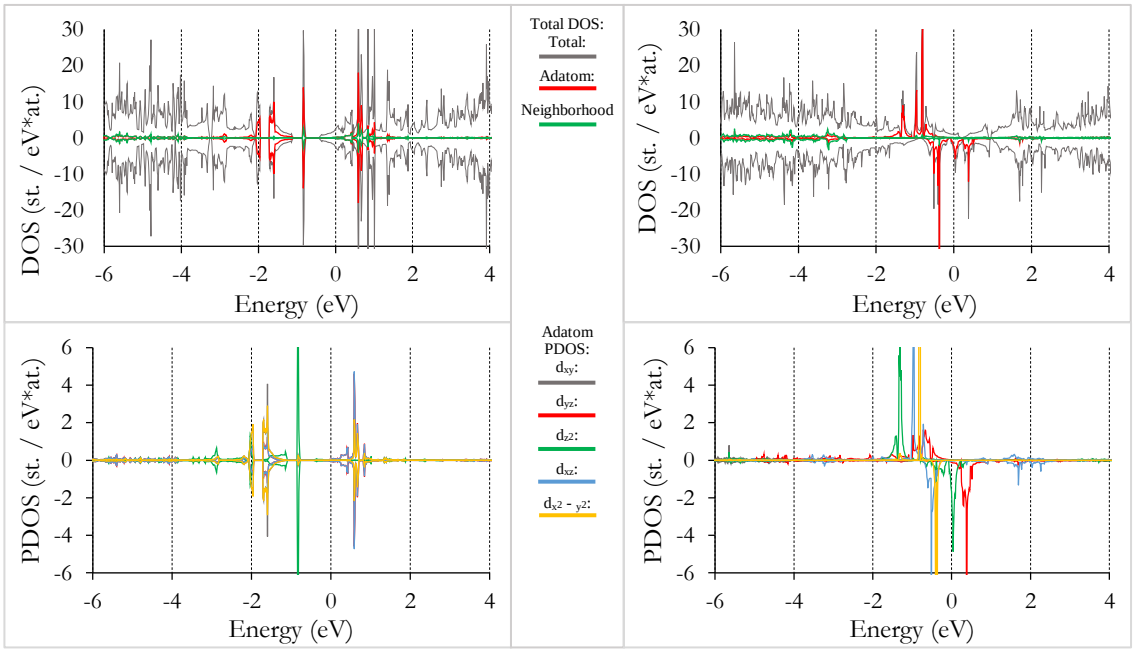

Adsorption energy: -4.915 eV
Total magnetic moment: 0.000 μ_B
Adatom magnetic moment: -0.000 μ_B
Graphene magnetic moment: 0.000 μ_B
Second biggest magnetic moment: 0.000 μ_B

RuDVNG

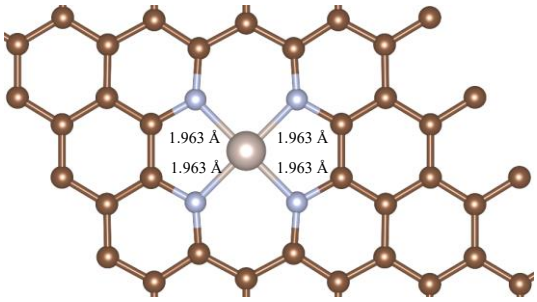

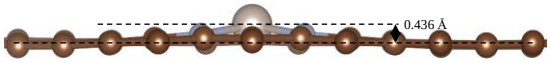

Adsorption energy: -7.141 eV
Total magnetic moment: 1.708 μ_B
Adatom magnetic moment: 1.274 μ_B
Graphene magnetic moment: 0.147 μ_B
Second biggest magnetic moment: 0.018 μ_B

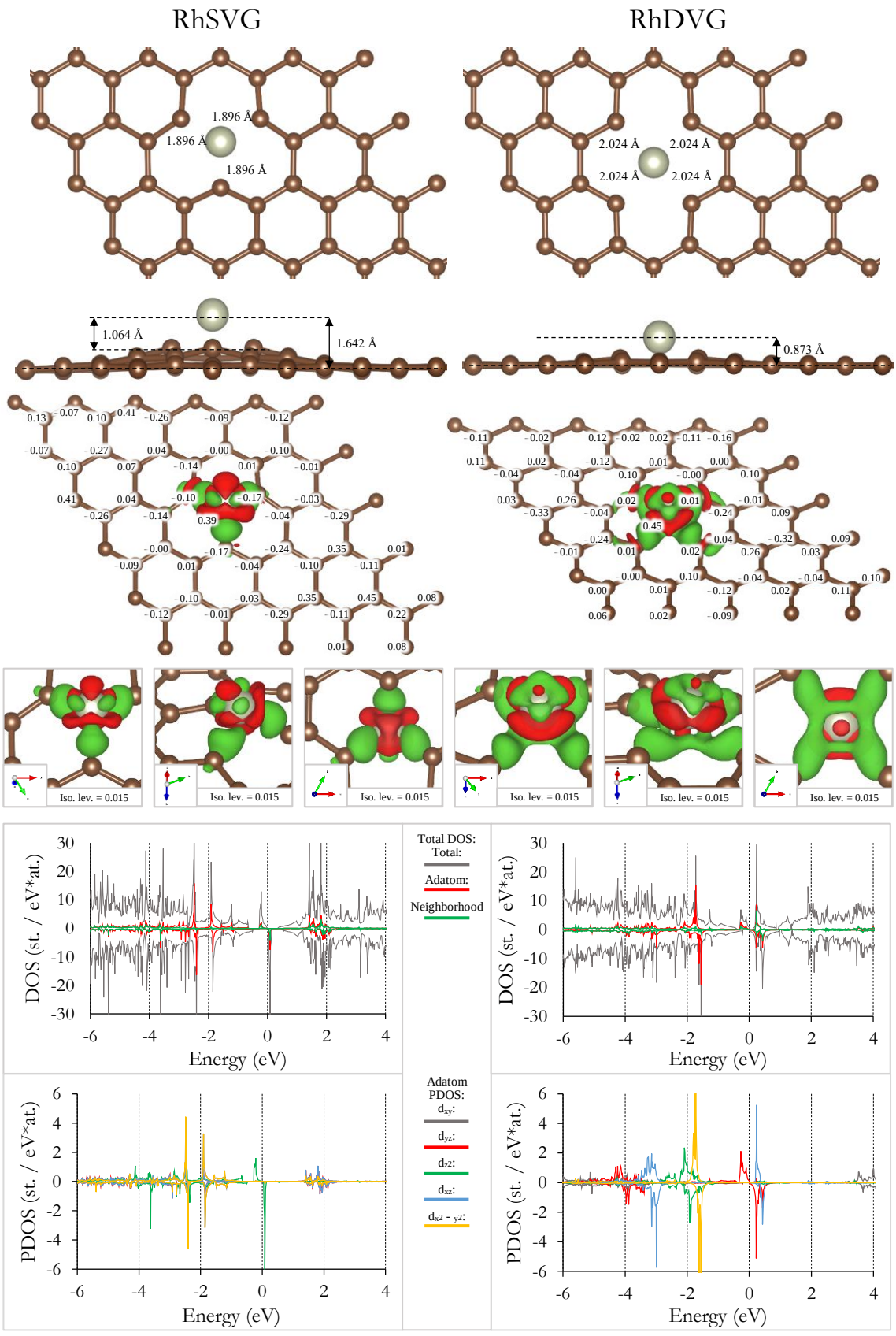

Adsorption energy: -8.179 eV
Total magnetic moment: 1.000 μ_B
Adatom magnetic moment: 0.204 μ_B
Graphene magnetic moment: 0.368 μ_B
Second biggest magnetic moment: 0.052 μ_B

Adsorption energy: -7.039 eV
Total magnetic moment: 0.988 μ_B
Adatom magnetic moment: 0.475 μ_B
Graphene magnetic moment: 0.251 μ_B
Second biggest magnetic moment: 0.036 μ_B

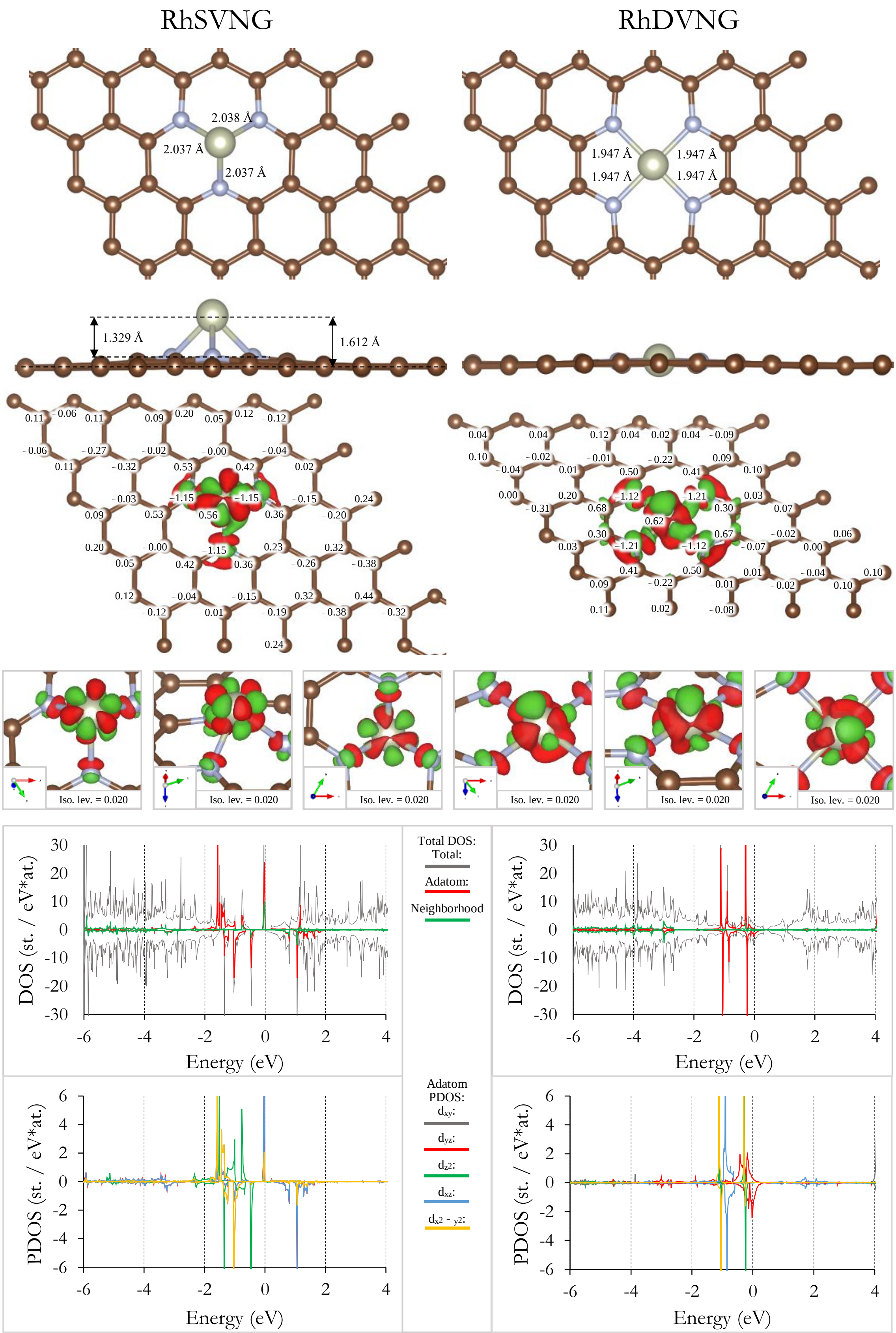

Adsorption energy: -4.073 eV
Total magnetic moment: 2.000 μB
Adatom magnetic moment: 0.978 μB
Graphene magnetic moment: 0.580 μB
Second biggest magnetic moment: 0.121 μB

Adsorption energy: -7.375 eV
Total magnetic moment: 0.253 μB
Adatom magnetic moment: 0.155 μB
Graphene magnetic moment: 0.051 μB
Second biggest magnetic moment: 0.006 μB

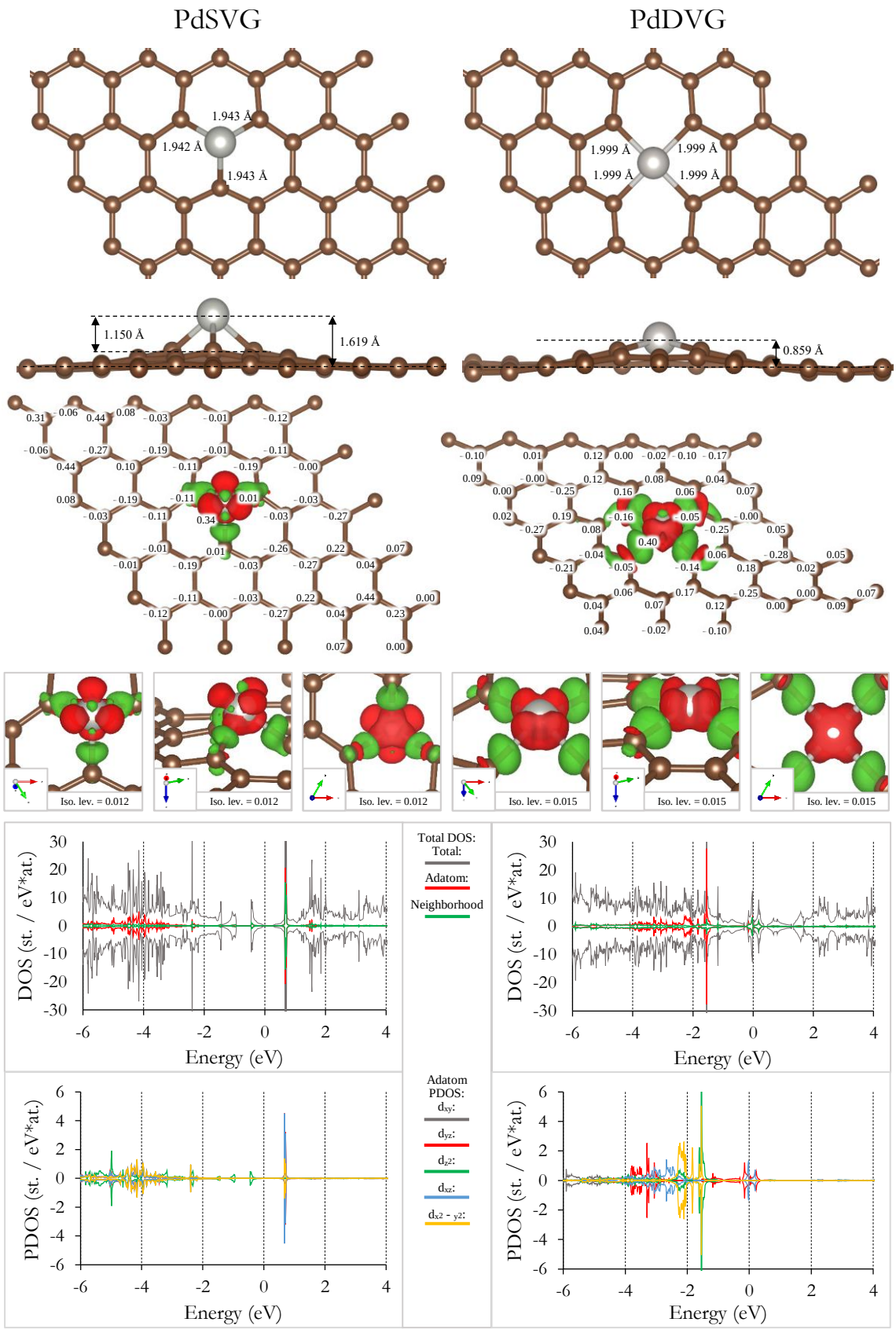

Adsorption energy: -5.283 eV
Total magnetic moment: 0.000 μ_B
Adatom magnetic moment: 0.000 μ_B
Graphene magnetic moment: 0.000 μ_B
Second biggest magnetic moment: 0.000 μ_B

Adsorption energy: -4.705 eV
Total magnetic moment: -0.000 μ_B
Adatom magnetic moment: 0.000 μ_B
Graphene magnetic moment: 0.000 μ_B
Second biggest magnetic moment: 0.000 μ_B

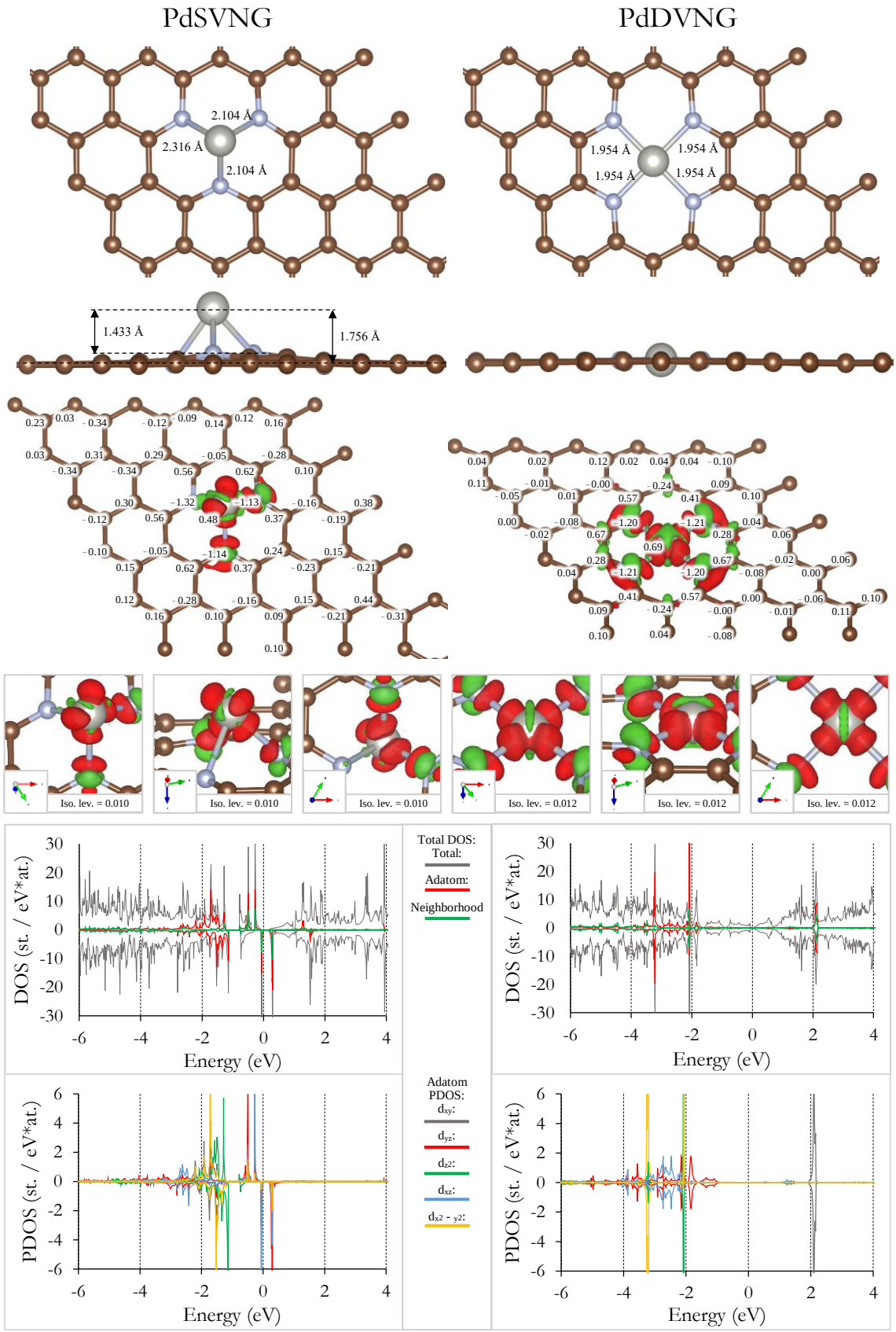

Adsorption energy: -2.383 eV
Total magnetic moment: 1.000 μ_B
Adatom magnetic moment: 0.543 μ_B
Graphene magnetic moment: 0.134 μ_B
Second biggest magnetic moment: 0.134 μ_B

Adsorption energy: -5.808 eV
Total magnetic moment: 0.000 μ_B
Adatom magnetic moment: -0.000 μ_B
Graphene magnetic moment: 0.000 μ_B
Second biggest magnetic moment: 0.000 μ_B

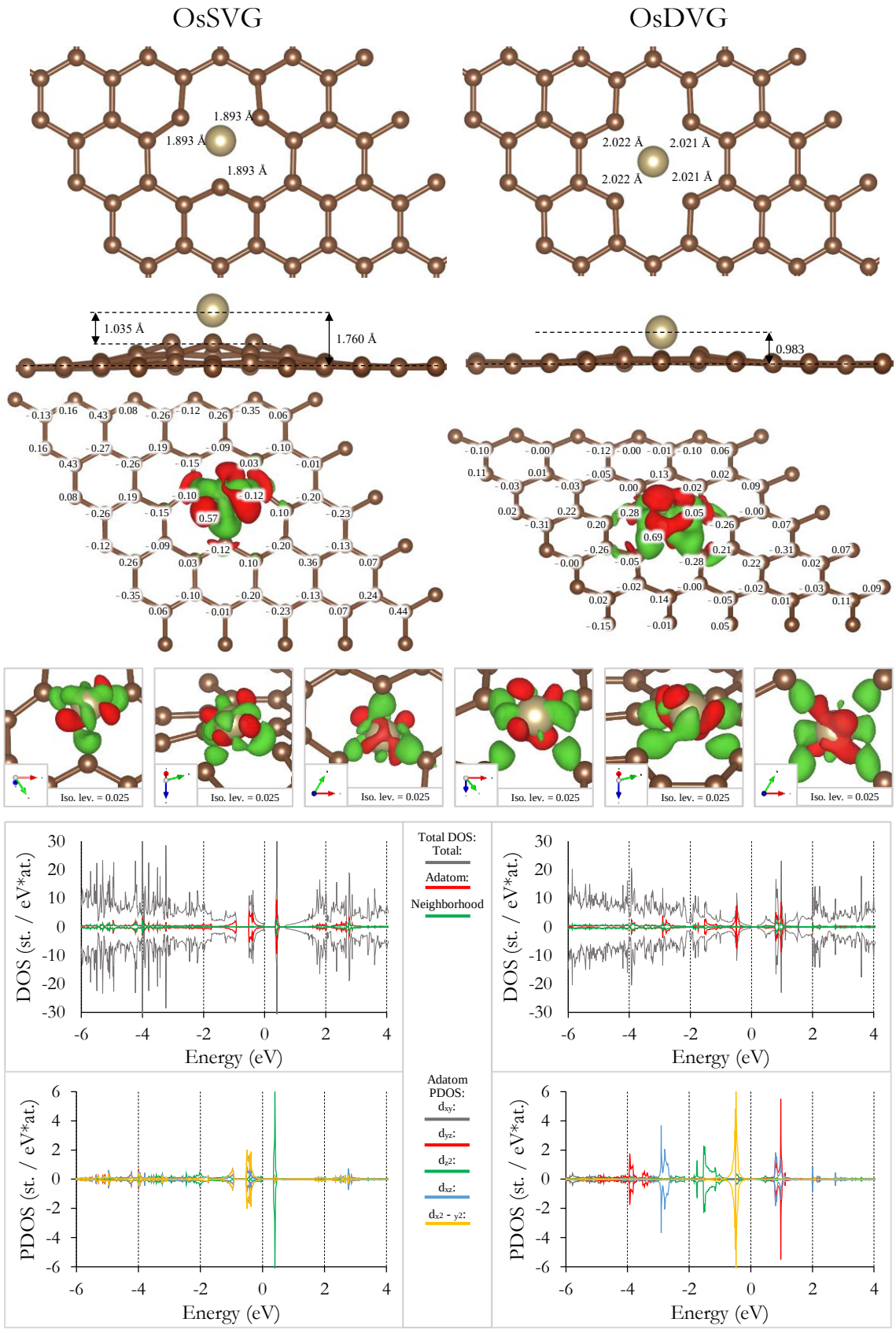

Adsorption energy: -9.394 eV
Total magnetic moment: 0.000 μ_B
Adatom magnetic moment: -0.000 μ_B
Graphene magnetic moment: 0.000 μ_B
Second biggest magnetic moment: 0.000 μ_B

Adsorption energy: -9.110 eV
Total magnetic moment: 0.000 μ_B
Adatom magnetic moment: 0.000 μ_B
Graphene magnetic moment: 0.000 μ_B
Second biggest magnetic moment: 0.000 μ_B

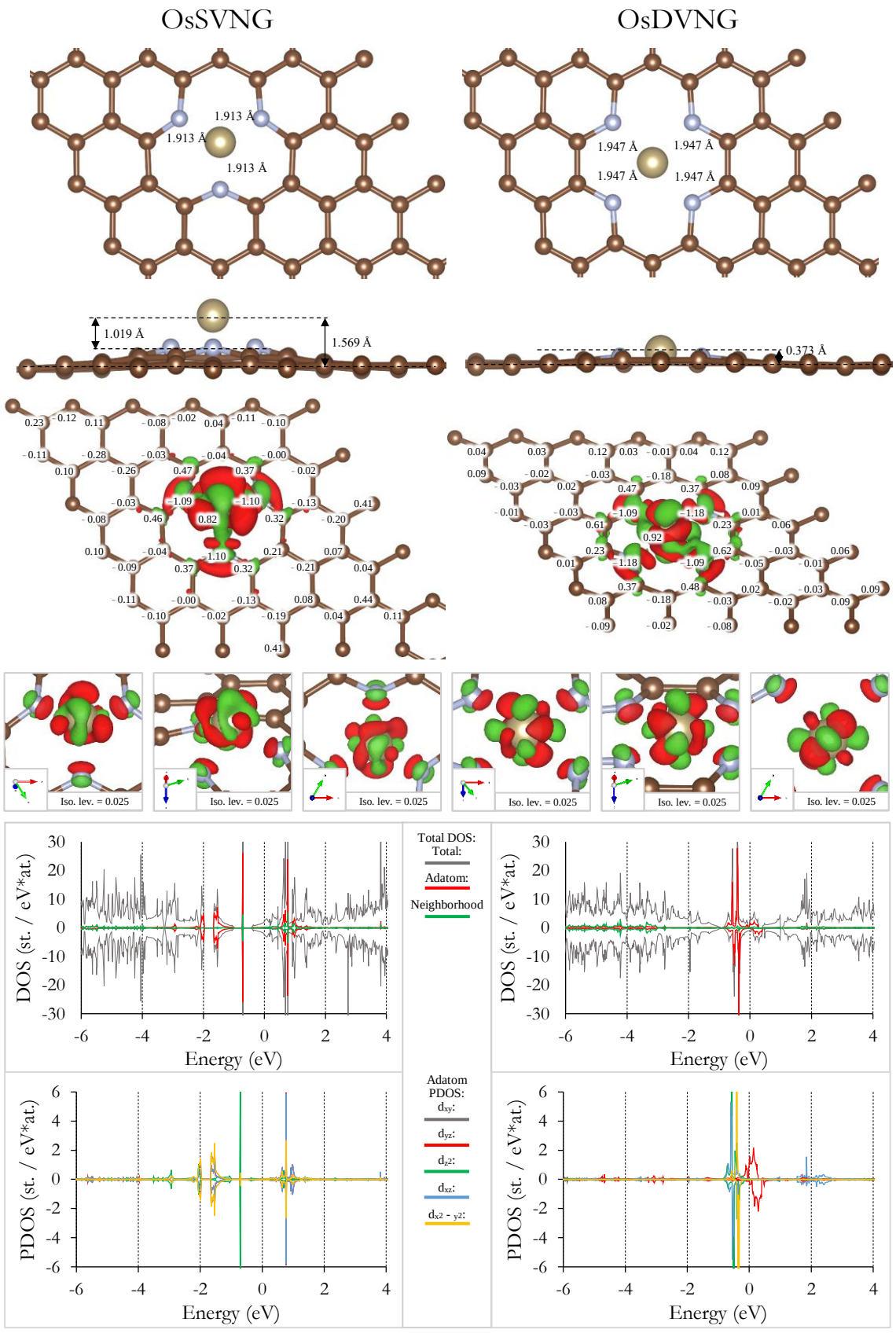

Adsorption energy: -4.818 eV
Total magnetic moment: 0.000 μ_B
Adatom magnetic moment: -0.000 μ_B
Graphene magnetic moment: 0.000 μ_B
Second biggest magnetic moment: 0.000 μ_B

Adsorption energy: -7.784 eV
Total magnetic moment: 0.146 μ_B
Adatom magnetic moment: 0.154 μ_B
Graphene magnetic moment: -0.014 μ_B
Second biggest magnetic moment: -0.004 μ_B

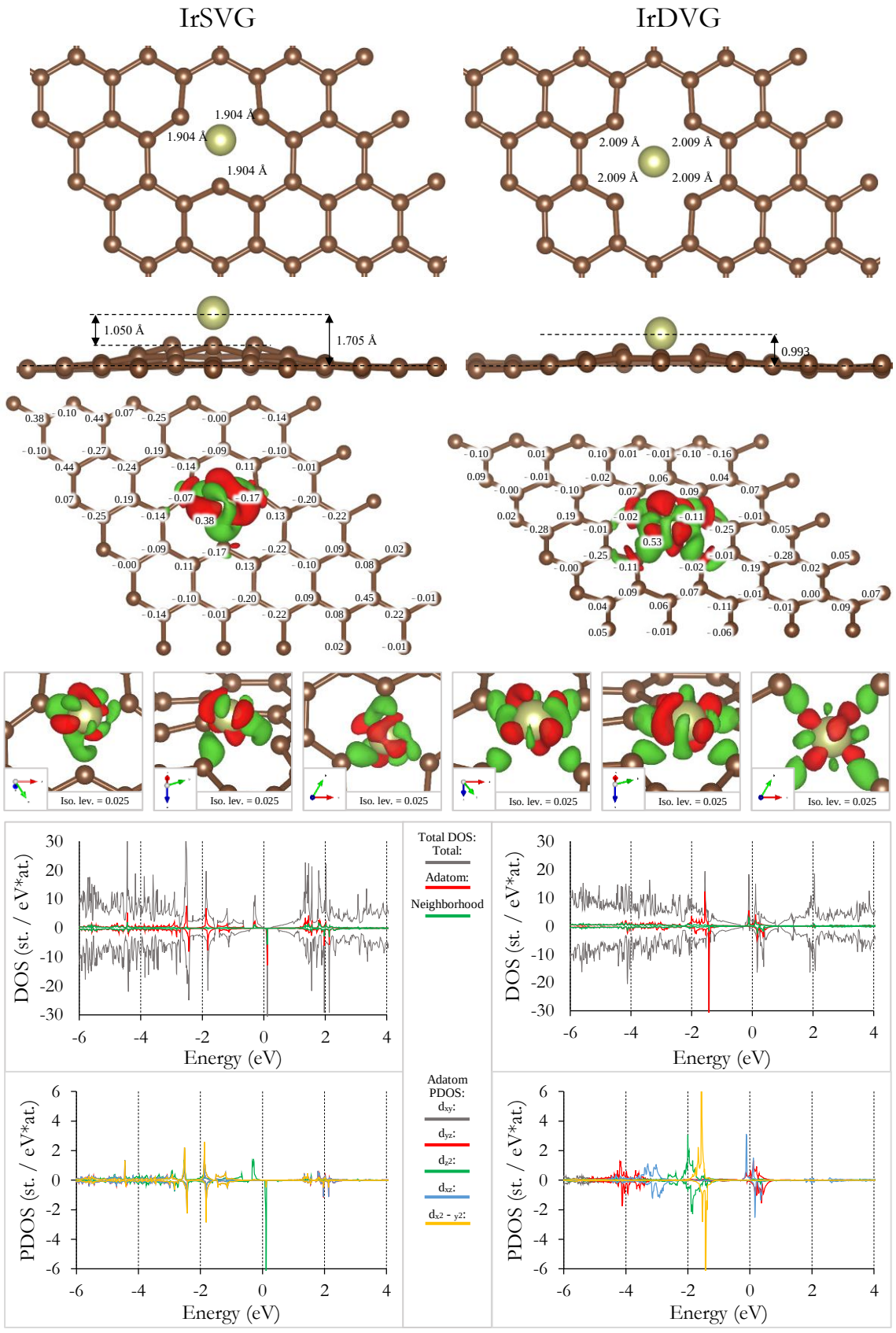

Adsorption energy: -9.165 eV
Total magnetic moment: 1.000 μ_B
Adatom magnetic moment: 0.265 μ_B
Graphene magnetic moment: 0.299 μ_B
Second biggest magnetic moment: 0.048 μ_B

Adsorption energy: -8.541 eV
Total magnetic moment: 0.852 μ_B
Adatom magnetic moment: 0.353 μ_B
Graphene magnetic moment: 0.269 μ_B
Second biggest magnetic moment: 0.035 μ_B

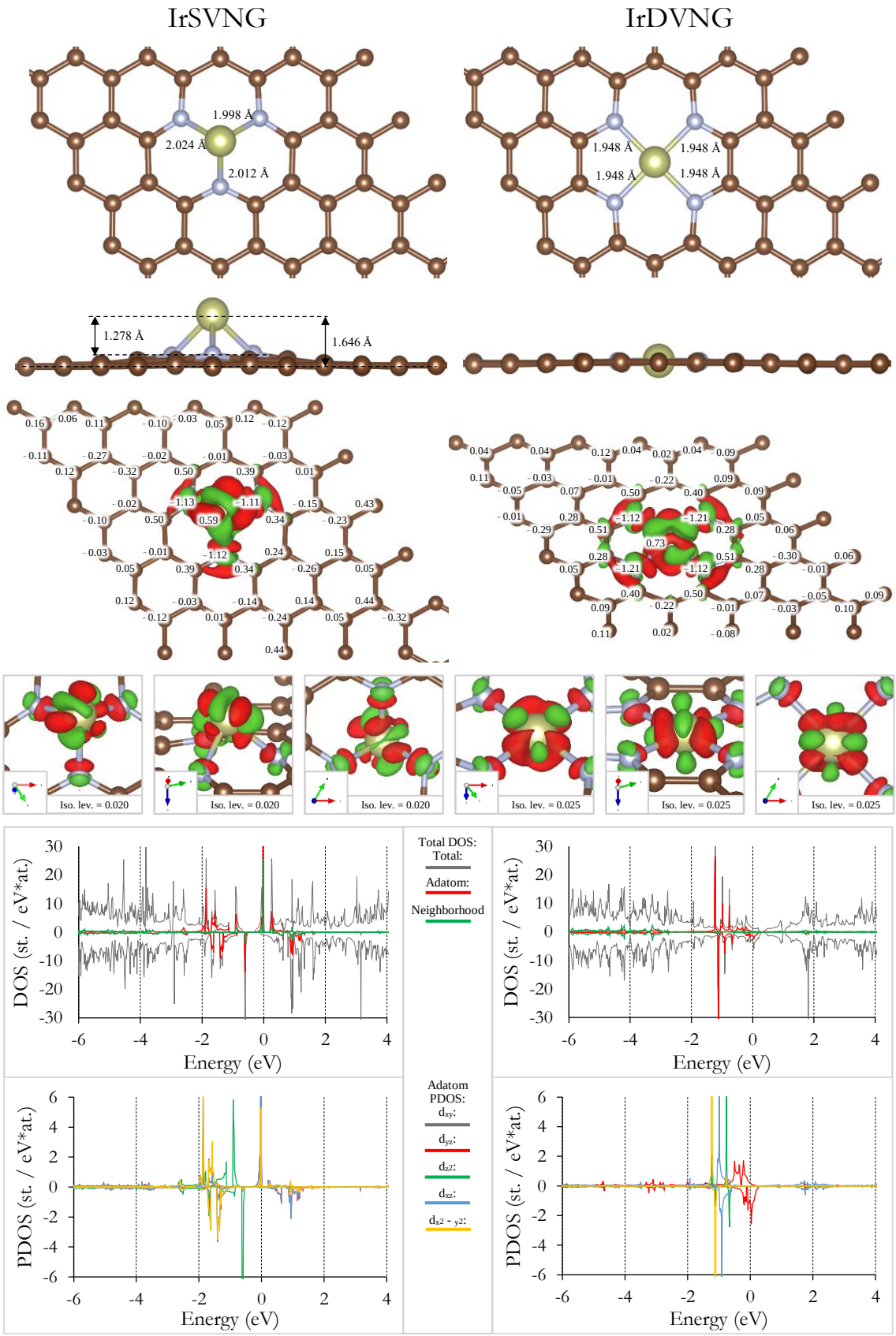

Adsorption energy: -3.970 eV
Total magnetic moment: 1.827 μ_B
Adatom magnetic moment: 0.740 μ_B
Graphene magnetic moment: 0.551 μ_B
Second biggest magnetic moment: 0.105 μ_B

Adsorption energy: -8.402 eV
Total magnetic moment: 0.480 μ_B
Adatom magnetic moment: 0.279 μ_B
Graphene magnetic moment: 0.105 μ_B
Second biggest magnetic moment: 0.010 μ_B

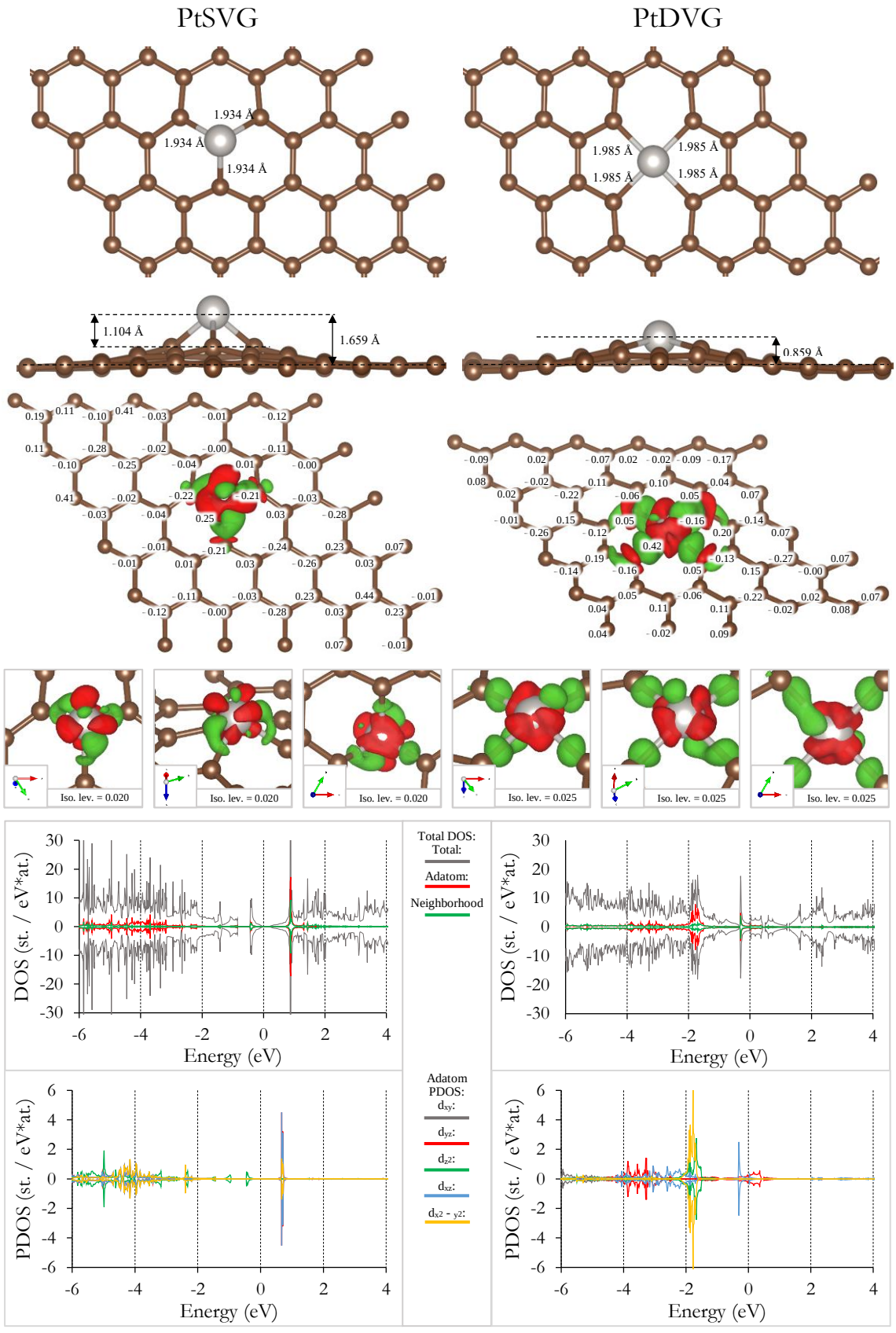

Adsorption energy: -7.166 eV
Total magnetic moment: -0.000 μ_B
Adatom magnetic moment: 0.000 μ_B
Graphene magnetic moment: 0.000 μ_B
Second biggest magnetic moment: 0.000 μ_B

Adsorption energy: -7.328 eV
Total magnetic moment: 0.000 μ_B
Adatom magnetic moment: 0.000 μ_B
Graphene magnetic moment: 0.000 μ_B
Second biggest magnetic moment: 0.000 μ_B

PtSVNG

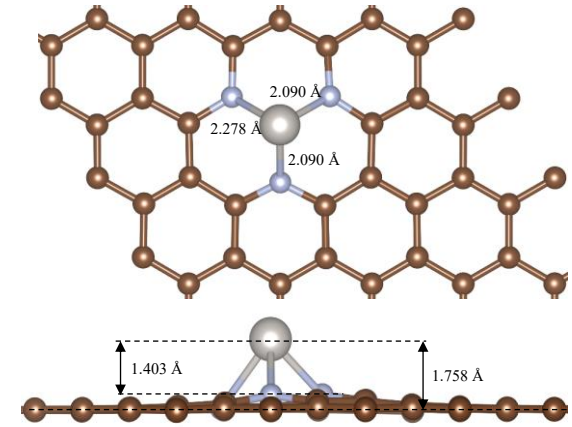

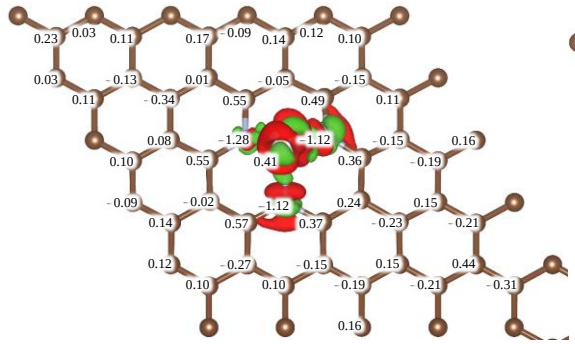

PtDVNG

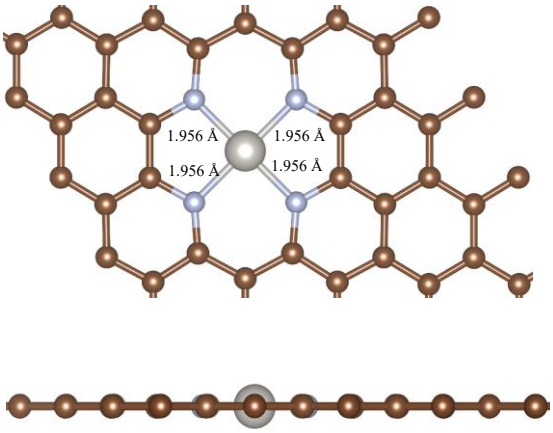

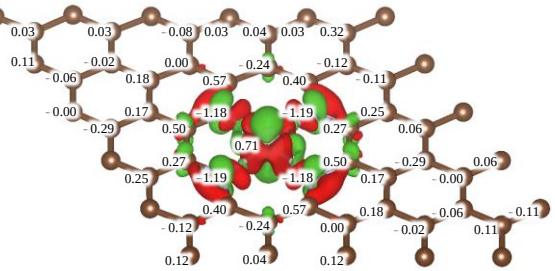

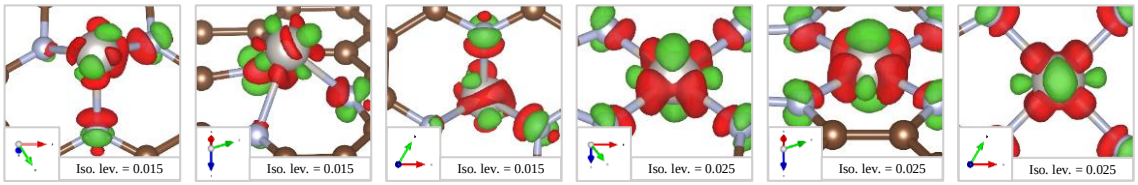

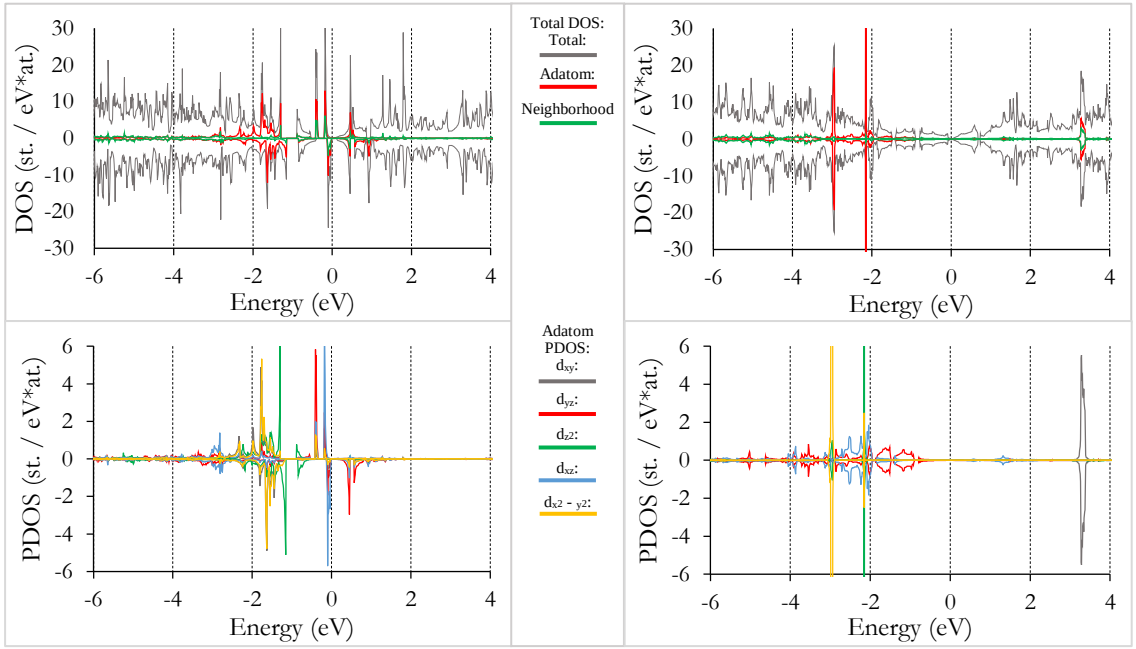

Adsorption energy: -2.874 eV
Total magnetic moment: 1.000 μ_B
Adatom magnetic moment: 0.533 μ_B
Graphene magnetic moment: 0.290 μ_B
Second biggest magnetic moment: 0.130 μ_B

Adsorption energy: -7.717 eV
Total magnetic moment: -0.000 μ_B
Adatom magnetic moment: 0.000 μ_B
Graphene magnetic moment: 0.000 μ_B
Second biggest magnetic moment: 0.000 μ_B